19. Konishi, K., Kojima, S., Katoh, T., Yazawa, M., Kato, K., Fujiwara, K., and Onishi, H. (2001) Two new modes of smooth muscle myosin regulation by the interaction between the two regulatory light chains, and by the S2 domain, *J. Biochem. 129*, 365−372.
20. Onishi, H., Maéda, K., Maéda, Y., Inoue, A., and Fujiwara, K. (1995) Functional chicken gizzard heavy meromyosin expression in and purification from baculovirus-infected insect cells, *Proc. Natl. Acad. Sci. U.S.A. 92*, 704−708.
21. Suzuki, Y., Yasunaga, T., Ohkura, R., Wakabayashi, T., and Sutoh, K. (1998) Swing of the lever arm of a myosin motor at the isomerization and phosphate-release steps, *Nature 396*, 380−383.
22. Stryer, L. (1978) Fluorescence energy transfer as a spectroscopic ruler, *Annu. Rev. Biochem. 47*, 819−846.
23. Finer, J. T., Simmons, R. M., and Spudich, J. A. (1994) Single myosin molecule mechanics: piconewton forces and nanometre steps, *Nature 368*, 113−119.
24. Molloy, J. E., Burns, J. E., Kendrick-Jones, J., Tregear, R. T., and White, D. C. (1995) Movement and force produced by a single myosin head, *Nature 378*, 209−212.
25. Hiratsuka, T. (1983) New ribose-modified fluorescent analogs of adenine and guanine nucleotides available as substrates for various enzymes, *Biochim. Biophys. Acta 742*, 496−508.
26. Batra, R., and Manstein, D. J. (1999) Functional characterization of *Dictyostelium* myosin II with conserved tryptophanyl residue 501 mutated to tyrosine, *Biol. Chem. 380*, 1017−1023.
27. Onishi, H., Konishi, K., Fujiwara, K., Hayakawa, K., Tanokura, M., Martinez, H. M., and Morales, M. F. (2000) On the tryptophan residue of smooth muscle myosin that responds to binding of nucleotide, *Proc. Natl. Acad. Sci. U.S.A. 97*, 11203−11208.
28. Marston, S. B., and Taylor, E. W. (1980) Comparison of the myosin and actomyosin ATPase mechanisms of the four types of vertebrate muscles, *J. Mol. Biol. 139*, 573−600.
29. Majoul, I., Straub, M., Duden, R., Hell, S. W., and Soling, H. D. (2002) Fluorescence resonance energy transfer analysis of protein−protein interactions in single living cells by multifocal multiphoton microscopy, *J. Biotechnol. 82*, 267−277.
30. Harada, Y., Noguchi, A., Kishino, A., and Yanagida, T. (1987) Sliding movement of single actin filaments on one-headed myosin filaments, *Nature 326*, 805−808.
31. Kron, S. J., and Spudich, J. A. (1986) Fluorescent actin filaments move on myosin fixed to a glass surface, *Proc. Natl. Acad. Sci. U.S.A. 83*, 6272−6276.
32. Gulick, A. M., Bauer, C. B., Thoden, J. B., and Rayment, I. (1997) X-ray structures of the MgADP, MgATPγS, and MgAMPPNP complexes of the *Dictyostelium discoideum* myosin motor domain, *Biochemistry 36*, 11619−11628.
33. Bauer, C. B., Holden, H. M., Thoden, J. B., Smith, R., and Rayment, I. (2000) X-ray structures of the apo and MgATP-bound states of *Dictyostelium discoideum* myosin motor domain, *J. Biol. Chem. 275*, 38494−38499.
34. Fisher, A. J., Smith, C. A., Thoden, J., Smith, R., Sutoh, K., Holden, H. M., and Rayment, I. (1995) Structural studies of myosin:nucleotide complexes: a revised model for the molecular basis of muscle contraction, *Biophys. J. 68*, 19S−26S.

BI048954F

THE JOURNAL OF BIOLOGICAL CHEMISTRY
Vol. 279, No. 38, Issue of September 17, pp. 40091–40099, 2004
Printed in U.S.A.

A Novel Dynamin-associating Molecule, Formin-binding Protein 17, Induces Tubular Membrane Invaginations and Participates in Endocytosis*[S]

Received for publication, May 3, 2004, and in revised form, June 17, 2004
Published, JBC Papers in Press, July 12, 2004, DOI 10.1074/jbc.M404899200

Yuji Kamioka‡, Shigetomo Fukuhara‡, Hirofumi Sawa§, Kazuo Nagashima§, Michitaka Masuda‡, Michiyuki Matsuda¶, and Naoki Mochizuki‡‖

From the ‡Department of Structural Analysis, National Cardiovascular Center Research Institute, 5-7-1 Fujishirodai, Suita, Osaka 565-8565, Japan, the §Laboratory of Molecular and Cellular Pathology, Hokkaido University School of Medicine, Sapporo 060-8638, Japan, and the ¶Department of Tumor Virology, Research Institute for Microbial Disease, Osaka University, Osaka 565-0871, Japan

Dynamin associates with a variety of SH3 domain-containing molecules via a C-terminal proline-rich motif and takes part, with them, in endocytic processes. Here, we have investigated a new dynamin-associating molecule, formin-binding protein 17 (FBP17), involved in deforming the plasma membrane and in endocytosis. FBP17 formed tubular invaginations originating from the plasma membrane. Its N-terminal Fer/CIP4 homology domain, a coiled-coil domain, and a proline-rich motif were required for tubular invagination and self-assembly, by which tubular invagination might be induced. Using anti-FBP17 antibody, we detected positive immunoreactions in the testis that were restricted to the germ cells. We also detected FBP17 in the brain by immunoblotting and *in situ* hybridization. When COS cells expressing enhanced green fluorescent protein-tagged FBP17 were incubated with fluorescently labeled transferrin, epidermal growth factor, and cholera toxin, these molecules co-localized with FBP17-induced tubular invaginations, suggesting that FBP17 is involved in dynamin-mediated endocytosis in both a clathrin-dependent and -independent manner. These observations therefore indicate that FBP17 interacts with dynamin and regulates endocytosis by forming vesicotubular structures.

The plasma membrane changes its structure dynamically in response to a wide variety of extracellular stimuli that alter cell shape. Membrane extension, including the formation of filopodia and lamellipodia, is controlled by the Rho family GTPases Cdc42 and Rac, respectively (1). Rac and Cdc42 are involved in forming membrane protrusions essential for phagocytosis and macropinocytosis (2), whereas another GTPase, dynamin, has been implicated in producing membrane invaginations and vesicles from the plasma membrane (3).

Dynamin is a multidomain GTPase; it consists of a GTPase domain followed by a central domain lacking homology to any other proteins, a pleckstrin homology domain, an effector domain, and a C-terminal proline-rich motif (4). Dynamin-1 (neuron-specific), dynamin-2 (ubiquitously expressed), and dynamin-3 (expressed only in the testis, brain, and lung), constitute the dynamin family (5–7). These proteins are essential for clathrin-dependent and also caveolae-mediated endocytosis (reviewed in Refs. 8 and 9). In addition, association of dynamin with Src homology 3 (SH3)[1] domain-containing molecules has been shown to modulate endocytosis since the C-terminal proline-rich motif provides an SH3 domain-binding site (10). The dynamin-binding molecules amphiphysin, endophilin, intersectin, and PACSIN/syndapin have been reported to be involved in modulating dynamin-dependent endocytosis (4, 11).

Formin-binding protein 17 (FBP17) consists of an N-terminal Fer/Cdc42-interacting protein 4 (CIP4) homology (FCH) domain followed by the first coiled-coil domain, a proline-rich motif, the second coiled-coil domain, a Rho family protein-binding domain (RBD), and a C-terminal SH3 domain. FBP17 was originally isolated as a molecule that binds to the proline-rich region of formin (12). FBP17 is fused to mixed-lineage leukemia in acute myeloid leukemia (13). However, its function remains unclear.

Based on domain structure, it is evident that FBP17 is closely related to CIP4. CIP4 localizes to microtubules presumably via its N-terminal FCH domain, binds to Cdc42 via the central region corresponding to the RBD of FBP17, and associates with Wiskott-Aldrich syndrome protein via a C-terminal SH3 domain (14). A CIP4 homolog, Rapostlin, consists of an N-terminal FCH domain, an RBD, and a C-terminal SH3 domain similar to CIP4. Rapostlin has been identified as an effector that binds to the Rho family GTPase Rnd2 (15). Rapostlin shares 93% amino acid identity with FBP17, indicating that FBP17 is likely to be an ortholog of Rapostlin. Like CIP4, Rapostlin partially localizes to microtubules via its N-terminal FCH domain (15). Although the FCH domain is thought to be a microtubule-targeting domain (16), we have previously shown

* This work was supported in part by grants from the Ministry of Health, Labor, and Welfare of Japan; the Promotion of Fundamental Studies in Health Science of the Organization for Pharmaceutical Safety and Research of Japan; the Ministry of Education, Science, Sports, and Culture of Japan; the Cell Science Research Foundation; the Uehara Memorial Foundation; and the Takeda Medical Research Foundation. The costs of publication of this article were defrayed in part by the payment of page charges. This article must therefore be hereby marked "*advertisement*" in accordance with 18 U.S.C. Section 1734 solely to indicate this fact.

[S] The on-line version of this article (available at http://www.jbc.org) contains Supplemental Figs. 1 and 2 and Videos 1 and 2.

‖ To whom correspondence should be addressed. Tel.: 81-6-6833-5012 (ext. 2508); Fax: 81-6-6835-5461; E-mail: nmochizu@ri.ncvc.go.jp.

[1] The abbreviations used are: SH3, Src homology 3; FBP17, formin-binding protein 17; CIP4, Cdc42-interacting protein 4; FCH, Fer/CIP4 homology; RBD, Rho family protein-binding domain; EGF, epidermal growth factor; CTB, cholera toxin subunit B; EGFP, enhanced green fluorescent protein; $DiIC_{16}(3)$, 1,1′-dihexadecyl-3,3,3′,3′-tetramethylindocarbocyanine perchlorate; GFP, green fluorescent protein; DMEM, Dulbecco's modified Eagle's medium; PBS, phosphate-buffered saline; GST, glutathione *S*-transferase; M-amphiphysin-2, muscle amphiphysin-2.

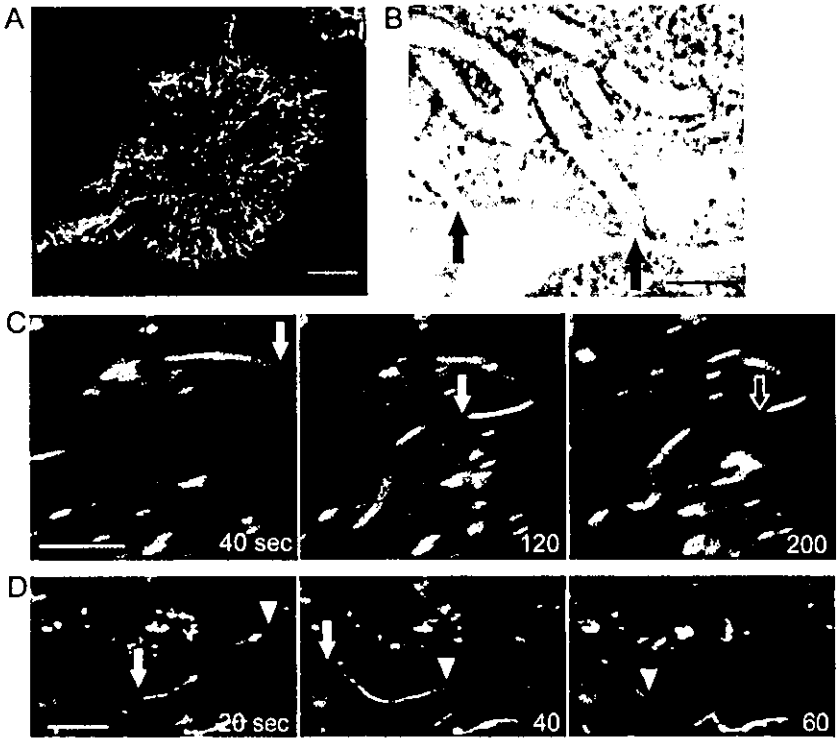

FIG. 1. **FBP17 generates tubules growing from the plasma membrane to inside of the cells.** *A*, COS-1 cells cultured on collagen-coated glass-bottom dishes were transfected with an EGFP-tagged FBP17-expressing plasmid. Cells were imaged on an Olympus IX-71 epifluorescence microscope. *Bar* = 10 μm. *B*, COS-1 cells expressing EGFP-tagged FBP17 was examined with a Hitachi H-800 electron microscope. Tubular structures originating from the plasma membrane were observed as indicated by the *arrows*. *Bar* = 1 μm. *C*, COS-1 cells expressing EGFP-tagged FBP17 were monitored by time-lapse imaging every 20 s. *Closed arrows* indicate the growth of cylindrical structure toward the inside of the cell. The *open arrow* denotes the retracting tubule in the cell. The time that elapsed from the beginning of the observation is shown at the right bottom of each panel. *Bar* = 5 μm. A series of these images has been converted to a video file (Supplemental Video 1). *D*, other COS-1 cells expressing EGFP-tagged FBP17 were monitored by time-lapse imaging. *Closed arrowheads* and *arrows* indicate the origin and the end of the tubule, respectively. Note that the tubule was internalized. A series of these images has been converted to a video file (Supplemental Video 2). *Bar* = 5 μm.

that the FCH domain of Fer tyrosine kinase is not required for localization of Fer to microtubules (17). In addition, the dynamin-associating molecule PACSIN/syndapin, which contains an N-terminal FCH domain, does not localize to microtubules (18). Since both FBP17 and PACSIN contain an N-terminal FCH domain, a coiled-coil domain, and a C-terminal SH3 domain, it seems probable that FBP17 is also involved in dynamin-regulated endocytosis.

In this study, we demonstrate that FBP17 induces the plasma membrane to form tubular structures and that FBP17 associates with a C-terminal proline-rich motif of dynamin. Transferrin, epidermal growth factor (EGF), and cholera toxin subunit B (CTB) are taken up along with FBP17-induced tubules in COS-1 cells expressing FBP17, suggesting that FBP17 is involved in dynamin-mediated endocytosis.

EXPERIMENTAL PROCEDURES

Plasmids—Full-length *FBP17* and *PACSIN-1* cDNAs were amplified by PCR from a human brain cDNA library (Clontech). PCR-amplified DNAs encoding FBP17 and its truncated mutants FBP17-N1 (amino acids 1–250), FBP17-N2 (amino acids 1–377), FBP17-C1 (amino acids 291–616), FBP17-dFCH (amino acids 80–616) were inserted into pCA-EGFP, a protein expression vector tagged at its N terminus with enhanced green fluorescent protein (EGFP) and derived from vector pCAGGS (19). A DNA fragment encoding a modified form of FBP17 referred to as FBP17-P597L, in which Leu is substituted for Pro^{597} in the SH3 domain, was amplified by PCR-based mutagenesis and ligated into pCA-EGFP. Full-length *PACSIN-1* cDNA was likewise inserted into pCA-EGFP. pCXN2-FLAG-FBP17-N2 is derived from pCAGGS and expresses N-terminally FLAG-tagged FBP17-N2. A cDNA encoding the SH3 motif of FBP17 (amino acids 534–616) and a cDNA encoding a nonfunctional SH3 domain (P597L) of FBP17 were amplified by PCR and ligated into pGEX-4T3 (Amersham Biosciences, Little Chalfont, Buckinghamshire, United Kingdom). Full-length *dynamin-1* and *dynamin-2* cDNAs were obtained by PCR from a human heart cDNA library and ligated into pCA-EGFP and pCXN2-FLAG. Full-length *dynamin-3* cDNA was amplified by PCR using KIAA0820 (a kind gift from Kazusa DNA Research Institute, Chiba, Japan) as a template and ligated into pEGFP-C1 (Clontech). cDNA encoding a GTPase-deficient mutant of dynamin-1 with Ala substituted for Lys^{44} (K44A) was amplified by PCR-based mutagenesis and ligated into pERed-NLS. pERed-NLS-dynamin-1-K44A expresses both FLAG-tagged dynamin-1-K44A and internal ribosomal entry signal-driven DsRed-Express fused with a nuclear localization signal (Clontech). pBluescript (Stratagene, La Jolla, CA) containing nucleotides 809–1851 of FBP17 was used to produce both antisense and sense riboprobes for *in situ* hybridization. All of the DNA fragments amplified by PCR were ligated into the pCR4blunt-TOPO vector (Invitrogen) and confirmed by sequencing with an Applied Biosystems ABI Prism 3700 sequencer.

Reagents and Antibodies—$DiIC_{16}(3)$, Alexa 546-conjugated transferrin, Texas Red-conjugated EGF, Alexa 555-conjugated CTB, Alexa 546-conjugated goat anti-mouse IgG, and Alexa 488-conjugated goat anti-rabbit IgG were purchased from Molecular Probes, Inc. (Eugene, OR). Anti-β-tubulin antibody, anti-vimentin antibody, rhodamine-conjugated phalloidin, and anti-FLAG antibody M2 were from Sigma. Anti-KDEL antibody was from Stressgen Biotech Corp. Anti-dynamin-2 antibody was from Santa Cruz Biotechnology (Santa Cruz, CA). Protein A-Sepharose, protein G-Sepharose, and glutathione-Sepharose from Amersham Biosciences. The digoxigenin-labeled riboprobe synthesis kit and the random-primed DNA labeling kit were from Roche Diagnostics (Basel, Switzerland). [α-^{32}P]dCTP (EasyTides™) was from PerkinElmer Life Sciences. Anti-green fluorescent protein (GFP) antibody was developed in our laboratory, and anti-FBP17 antibody was produced by immunizing rabbits with a keyhole limpet hemocyanin-coupled synthetic peptide (CAQDRESPDGSYTEEQSQES) corresponding to amino acids 506–525 of FBP17.

Cell Culture and Transfection—293T cells (a gift from B. J. Meyer, University of Connecticut, Storrs, CT) and COS-1 cells (American Type Culture Collection, Manassas, VA) were maintained in Dulbecco's modified Eagle's medium (DMEM) supplemented with 10% fetal

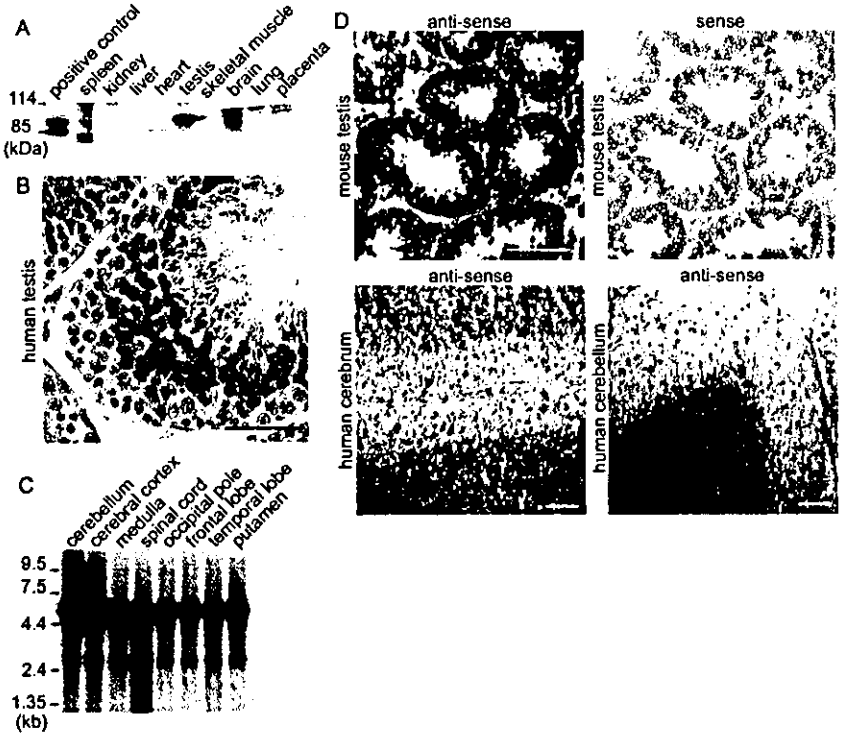

FIG. 2. **FBP17 is expressed in the testis and brain.** *A*, proteins from the mouse tissues indicated were subjected to SDS-PAGE followed by immunoblotting with anti-FBP17 antibody. A lysate of 293T cells expressing FLAG-tagged FBP17 was used as positive control. Molecular mass markers are on the left. *B*, the sections of human testis fixed with Bouin's solution were immunostained with anti-FBP17 antibody and visualized with diaminobenzidine (*brown*). Staining can be seen in all cells except those in the innermost and outermost layers. *Bar* = 50 μm. *C*, an RNA blot (human multiple-tissue blot) was probed with radiolabeled *FBP17* cDNA. 6.0-kb transcription products was detected in all lanes with RNAs prepared from the various regions of the brain as indicated. The detection procedure is described under "Experimental Procedures." *D*, frozen sections from the tissues indicated were probed with digoxigenin-labeled FBP17 antisense or sense probes. *FBP17* mRNA that hybridized with the probe appears *dark purple*. *Bars* = 200 μm.

bovine serum. Cells were transfected using LipofectAMINE 2000 (Invitrogen).

Cell Membrane Staining—COS-1 cells cultured on glass-bottom dishes were washed three times with DMEM without phenol red, incubated with DMEM containing 10 μg/ml $DiIC_{16}(3)$ for 10 min, rinsed twice with phosphate-buffered saline (PBS), fixed with 2% formaldehyde in PBS, and examined by confocal fluorescence imaging.

Transferrin, EGF, and CTB Uptake—COS-1 cells expressing EGFP-FBP17 were serum-starved in DMEM for 1 h and incubated with 25 μg/ml Alexa 546-conjugated transferrin for 20 min at either 37 °C or 4 °C and with 1 ng/ml Texas Red-conjugated EGF or 1 μg/ml Alexa 555-conjugated CTB at 37 °C. After rinsing three times with PBS and reducing surface labeling using 50 mM deferoxamine mesylate-containing buffer (150 mM NaCl, 2 mM $CaCl_2$, and 25 mM sodium acetate/acetic acid, pH 4.5), the cells were fixed with 2% formaldehyde in PBS and subjected to fluorescence imaging. Images of fluorescence-conjugated transferrin, EGF, or CTB were obtained with an Olympus IX-71 epifluorescence microscope equipped with a cooled charge-coupled camera (CoolSNAP-HQ, Roper Scientific, Trenton, NJ).

Immunoblotting and Immunoprecipitation—Immunoblotting and immunoprecipitation were performed as described previously (17). Briefly, 293T cells were washed with PBS and lysed with buffer containing 150 mM NaCl, 20 mM Tris-HCl (pH 7.5), 1.5 mM $MgCl_2$, 1% Triton X-100, and protease inhibitor mixture (Roche Diagnostics). Precleared cell lysates were immunoprecipitated with antibodies as indicated together with protein A- or G-Sepharose. Precipitates were subjected to SDS-PAGE followed by immunoblotting with antibodies as indicated. Proteins that reacted with the primary antibody recognized by the peroxidase-conjugated secondary antibody and that were species-matched were visualized with the ECL system (Amersham Biosciences) and a LAS-1000 image analyzer (Fuji Film, Tokyo, Japan). Tissues from BALB/c mice were rinsed with PBS and homogenized in lysis buffer (62.5 mM Tris-HCl (pH 6.8), 10% glycerol, 2% SDS, and bromphenol). The homogenates were centrifuged at 100,000 × *g* for 10 min. The pellets were fractionated by SDS-PAGE and immunoblotted with anti-FBP17 antibody.

Immunohistochemistry and Electron Microcopy—Human testis fixed with Bouin's solution and embedded in paraffin was sectioned, deparaffinized, and immunostained with anti-FBP17 antibody. Immunoreactivity detected by the peroxidase-conjugated secondary antibody was visualized with 1 mg/ml diaminobenzidine. Sections were counterstained with hematoxylin. For electron microscopy, COS-1 cells expressing EGFP-FBP17 were fixed with 2.5% glutaraldehyde and postfixed in 1% OsO_4 followed by embedding in epoxy resin. Ultrathin sections on nickel grids were immersed in target retrieval solution (DakoCytomation, Kyoto, Japan). After washing with distilled water and drying, sections were stained with both uranyl acetate and lead citrate and examined with a Hitachi H-800 electron microscope.

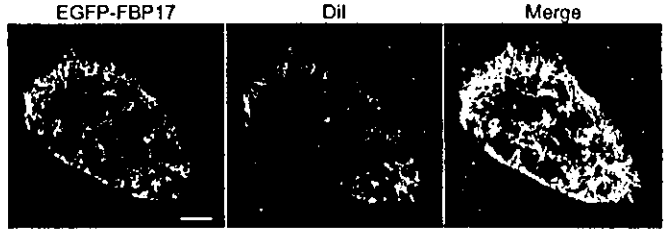

FIG. 3. **FBP17-induced tubular structures are plasma membrane invaginations.** COS-1 cells expressing EGFP-tagged FBP17 were incubated with $DiIC_{16}(3)$ for 10 min and fixed with PBS containing 2% formaldehyde. GFP images (*EGFP-FBP17*) and $DiIC_{16}(3)$-stained images (*DiI*) were obtained using an Olympus BX50EI confocal microscope and superimposed (*Merge*). *Bar* = 10 μm.

Northern Blot Analysis and in Situ Hybridization—A multiple-tissue Northern blot membrane (Human Brain II, Clontech) was prehybridized, followed by high stringency hybridization with an [α-^{32}P]dCTP-labeled FBP17 probe and washing with buffer containing appropriate concentrations of SSC and SDS. RNA hybridized with the radiolabeled probe was detected with a BAS-5000 imaging system (Fuji Film). *In situ* hybridization was performed as described previously (20). Briefly, mouse testis and human brain were embedded in Tissue-Tec OCT compound and frozen in liquid nitrogen. Cryostat sections were fixed in 4% paraformaldehyde, prehybridized, and hybridized overnight at 72 °C with digoxigenin-labeled riboprobe in hybridization buffer (50% formamide, 5× SSC, 5× Denhardt's solution, and 500 μg/ml tRNA). The sections were washed with 0.2× SSC and incubated with anti-digoxigenin antibody. The signal was visualized with nitro blue tetrazolium chloride/5-bromo-4-chloro-3-indolyl phosphate solution containing 0.24 mg/ml levamisole.

Confocal Microscopy and Fluorescence Imaging—Cells cultured on glass-bottom dishes and transfected with pCA-EGFP-FBP17 for 24 h were fixed with 2% formaldehyde and permeabilized with 0.1% Triton X-100. For anti-vimentin antibody immunostaining, cells were fixed with methanol. The permeabilized cells were incubated with anti-β-tubulin, anti-KDEL, or anti-vimentin antibody followed by Alexa 546-conjugated goat anti-mouse IgG to visualize tubulin, the endoplasmic reticulum, and vimentin. Actin was visualized with rhodamine-conjugated phalloidin. Fluorescent images of EGFP and of Alexa 546 or rhodamine were obtained with an Olympus BX50EI confocal microscope controlled by Fluoview (Olympus, Tokyo) as described previously

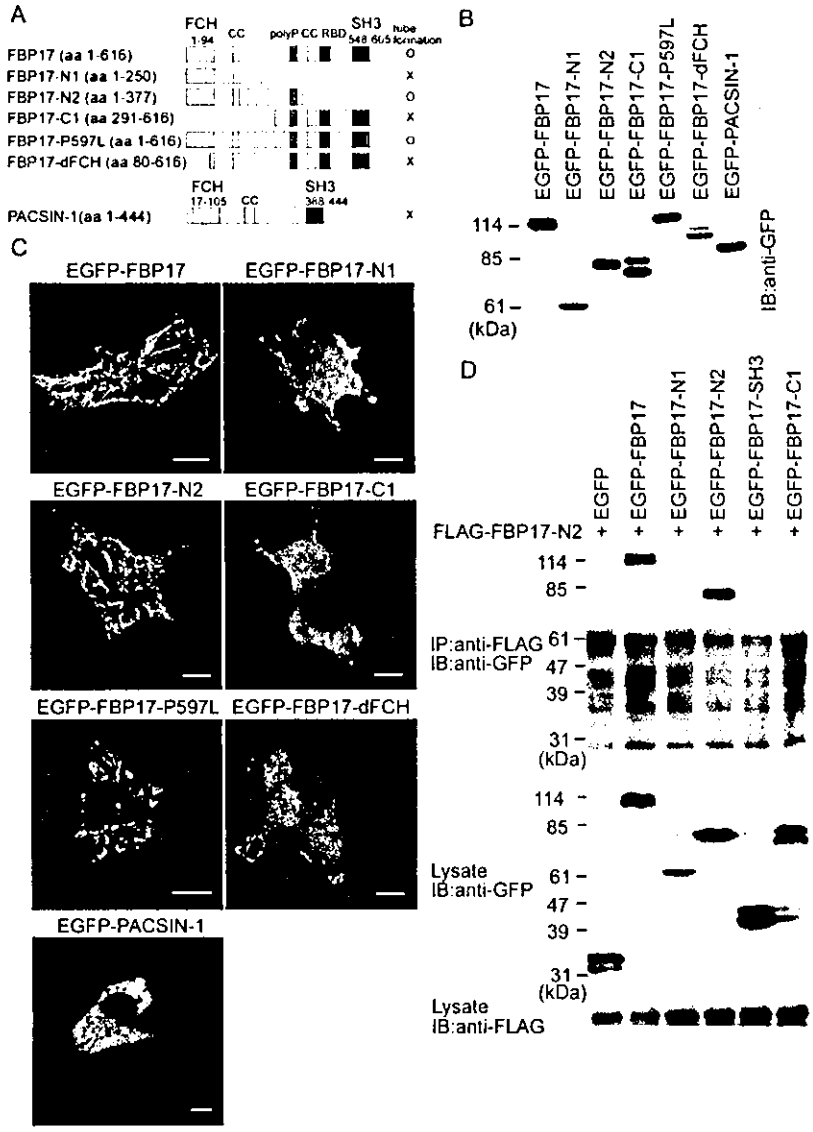

FIG. 4. **The N terminus of FBP17 is essential for FBP17-induced tubule formation.** *A*, shown is a schematic illustration of the structure of FBP17 consisting of an N-terminal FCH domain followed by a proline-rich motif (polyproline (*polyP*)) flanked by coiled-coil domains (*CC*), an RBD, and a C-terminal SH3 domain. Amino acid (*aa*) numbers are given on the left and at the top. Structurally related PACSIN-1 is indicated at the bottom. The results in *C* are summarized on the right. *B*, 293T cells were transfected with a plasmid expressing N-terminally EGFP-tagged proteins as indicated. Lysates of the transfectants were subjected to SDS-PAGE followed by immunoblotting with anti-GFP antibody. *C*, COS-1 cells transfected with the plasmids indicated were imaged by confocal microscopy (Olympus BX50EI). Note that essential domains required for tube formation are the FCH domain, the first coiled-coil domain, and the proline-rich motif. *Bars* = 10 μm. *D*, 293T cells were transfected with the plasmids indicated. Cell lysates were subjected either to immunoprecipitation (*IP*) followed by immunoblotting (*IB*) or directly to immunoblotting using the antibodies indicated. Note that the FCH domain, the first coiled-coil domain, and the polyproline motif are sufficient for dimerization of FBP17. The immunoblot results are representative of three independent experiments.

(21). Time-lapse fluorescence imaging was performed as described previously (21). Briefly, COS-1 cells expressing EGFP-FBP17 were cultured on a collagen-coated glass-bottom dish in DMEM/nutrient mixture F-12 (Invitrogen) supplemented with 10% fetal bovine serum, 2 mM L-glutamine, and 10 mM HEPES without phenol red. The cells were imaged using an Olympus IX-71 inverted microscope with a 75-watt xenon arc lamp equipped with a CoolSNAP-HQ cooled charge-coupled camera and two shutters, controlled by MetaMorph Version 5.0 software (Roper Scientific). To localize EGFP-tagged proteins, we obtained a fluorescent image every 20 s. Time-lapse images were converted to video format with MetaMorph Version 5.0 software.

Quantitative Analysis of the Effect of Dynamin-1-K44A on Internalization of FBP17-induced Tubules—To examine the effect of dynamin-1-K44A on FBP17-induced tubule formation, COS-1 cells were cotransfected with either pCA-EGFP-FBP17 or pCA-EGFP-FBP17-P597L and pERed-NLS-dynamin-1-K44A. Both EGFP images and DsRed images were obtained using an Olympus IX-71 epifluorescence microscope. EGFP intensity, which reflects the intracellular accumulation of all tubular invaginations that were not processed in the endocytic pathway, was calculated by measuring the total intensity of the cell divided by the total cell area using MetaMorph Version 5.0 software. Data obtained from 50 cells were averaged, and statistical significance was evaluated by Student's *t* test.

RESULTS

FBP17 Forms Tubular Invaginations in Living Cells—FBP17 has an N-terminal FCH domain. It has been suggested that this domain is a microtubule-targeting domain (16). Indeed, a previous study revealed that Rapostlin, a rat ortholog of human FBP17, partially localizes to microtubules (15). We therefore examined the localization of EGFP-tagged FBP17 in COS-1 cells (Fig. 1*A*) and found that it was located in cylindrical fiber structures of the cytoplasm. It was not present in the cytoskeleton, including microtubules, actin stress fibers, and intermediate filaments, or in the endoplasmic reticulum of COS-1 cells (Supplemental Fig. 1). When FLAG-tagged FBP17 was expressed in the cells, similar cylindrical fiber-like immunostaining was observed in the cytoplasm (Supplemental Fig. 2*B*).

We examined whether the cylindrical fiber structures are tubes. COS-1 cells transfected with a plasmid expressing EGFP-FBP17 were examined with an electron microscope. The open ends and the blind ends of the tubular structures induced by FBP17 were in the plasma membrane and cytoplasm, respectively (Fig. 1*B*). To examine how cylindrical fiber-like structure developed in the living cells, we monitored EGFP-FBP17 in COS-1 cells by time-lapse fluorescence microscopy. The fibers arose from the cell periphery, grew toward the center of the cell, and sometimes contracted back toward the periphery (Fig. 1*C* and Supplemental Video 1). We further noticed that some EGFP-FBP17-marked tubules were internalized instead of being contracted (Fig. 1*D* and Supplemental Video 2). The GFP-expressing plasmid used as a negative control did not induce any tubule formation. These results indicate

that FBP17 induces tubular plasma membrane invaginations.

FBP17 Is Expressed in the Brain and Testis—We developed an anti-FBP17 antibody and examined the expression of FBP17 in human and mouse organs and tissues. Immunoblot analysis revealed that FBP17 was expressed in mouse testis and brain (Fig. 2*A*). We then examined the localization of FBP17 in the seminiferous tubules of human testis by immunohistochemistry. Germ cells were immunoreactive to anti-FBP17 antibody, whereas Sertoli's cells were negative. Of the germ cells, the secondary spermatocytes in the inner layer of the tubules exhibited strong immunoreactivity, whereas spermatogonia in the outermost layer and spermatozoa in the innermost layer showed no immunoreactivity (Fig. 2*B*). This suggests that the expression of FBP17 is correlated with the maturation of germ cells. More detailed examination of the maturation stages revealed that germ cells, from secondary spermatocytes to elongated spermatids, were immunoreactive.[2]

We next asked whether FBP17 is expressed in the brain. Expression was examined by both Northern blot analysis and *in situ* hybridization. *FBP17* mRNA was detected as a transcript of ~6.0 kb in all regions of the human brain (Fig. 2*C*). It was also detected *in situ* in mouse testis and in the cortex of the cerebrum and in the granular layer of the cerebellum of human brain (Fig. 2*D*).

FBP17-induced Invagination Originating from the Plasma Membrane—To examine whether FBP17-induced tubules are continuous with the plasma membrane, we used $DiIC_{16}(3)$. $DiIC_{16}(3)$ is a lipophilic fluorescent probe used for plasma membrane staining (22). COS-1 cells expressing EGFP-tagged FBP17 were stained for $DiIC_{16}(3)$ and imaged for fluorescence (Fig. 3). EGFP-FBP17 expression and $DiIC_{16}(3)$ staining overlapped, supporting the idea that FBP17-generated tubules arise from the plasma membrane.

The C-terminal SH3 Domain Is Not Required for FBP17-induced Tubular Invagination—To investigate the mechanism by which tubular invagination is induced by FBP17, we constructed a series of deletion or point mutants of EGFP-tagged FBP17 (Fig. 4*A*). We confirmed that the EGFP-tagged mutants were correctly constructed, as they had the expected molecular mass in immunoblots probed with anti-GFP antibody (Fig. 4*B*). Full-length FBP17 and an SH3 domain mutant (FBP17-P597L) formed tubular structures (Fig. 4*C*), as did a derivative (FBP17-N2) with a deletion of the second coiled-coil region, the RBD, and the SH3 domain. In contrast, removal of the FCH domain in FBP17-dFCH or of both the FCH domain and the first coiled-coil domain in FBP17-C1 abolished tube formation. In addition, FBP17-N1, a derivative containing only the FCH domain and the first coiled-coil domain, was incapable of inducing tube formation. These results indicate that the FCH domain, the first coiled-coil domain, and the proline-rich region are essential for FBP17-induced tube formation. We also tested whether PACSIN-1, a molecule structurally related to FBP17, forms tubules like FBP17. Although PACSIN-1, like FBP17, contains an FCH domain followed by a coiled-coil domain and a C-terminal SH3 domain, it did not generate tubular structure, in agreement with a previous report (23).

We hypothesized that the self-assembly might contribute to the tube formation by FBP17. To test for self-assembly of FBP17, we expressed EGFP-tagged FBP17 and FLAG-tagged FBP17-N2 in 293T cells and examined their possible association by immunoprecipitation. Both EGFP-tagged full-length FBP17 and EGFP-tagged FBP17-N2 were co-immunoprecipitated with FLAG-tagged FBP17-N2 (Fig. 4*D*, *second* and *fourth lanes*), whereas EGFP-tagged FBP17-N1, FBP17-C1, and

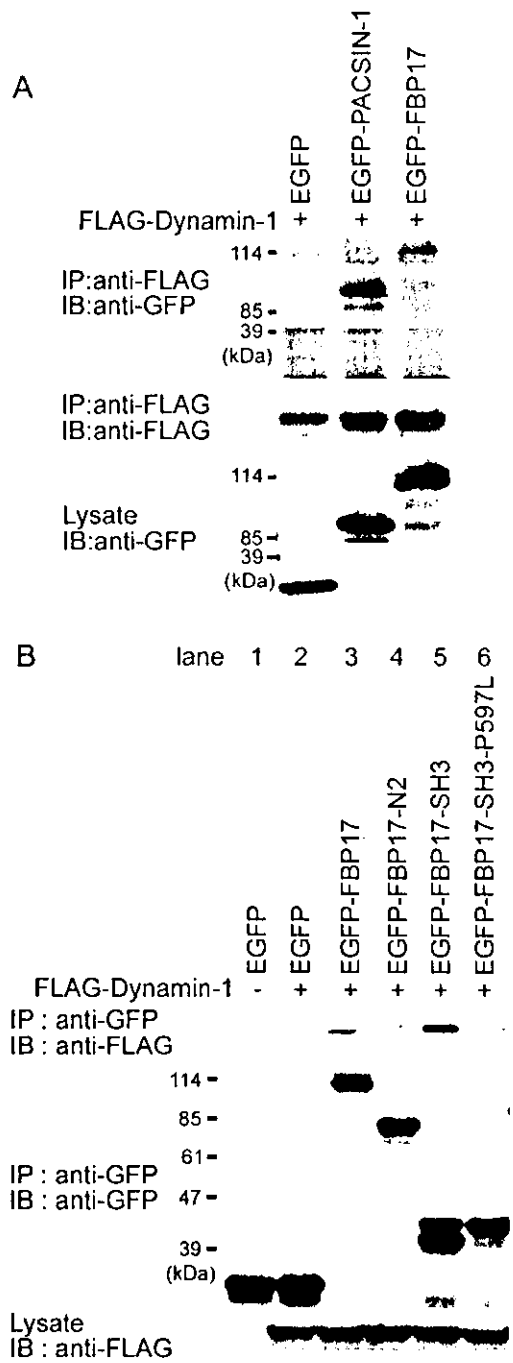

FIG. 5. **FBP17 associates with dynamin-1 in an SH3 domain-dependent manner.** *A*, 293T cells were transfected with the plasmids indicated. Cell lysates were subjected either to immunoprecipitation (*IP*) followed by immunoblotting (*IB*) or directly to immunoblotting using the antibodies indicated. PACSIN-1 was a positive control. *B*, the EGFP-tagged truncated mutants of FBP17 (FBP17-N2 and FBP17-SH3) and a nonfunctional SH3 mutant of FBP17 (FBP17-SH3-P597L) were analyzed for association with FLAG-tagged dynamin-1 as described for *A*. The immunoblots are representative of more than three independent experiments.

FBP17-SH3 were not co-immunoprecipitated. These results indicate that the FCH domain followed by a coiled-coil domain and polyproline regions are required for self-assembly.

FBP17 Associates with Dynamin via Its SH3 Domain—PACSIN-1 and its rat ortholog, syndapin, are involved in clathrin-mediated endocytosis through an association with dynamin via their C-terminal SH3 domains (24). We tested whether FBP17 associates with dynamin because FBP17 contains an

[2] Y. Kamioka, H. Sawa, and N. Mochizuki, unpublished data.

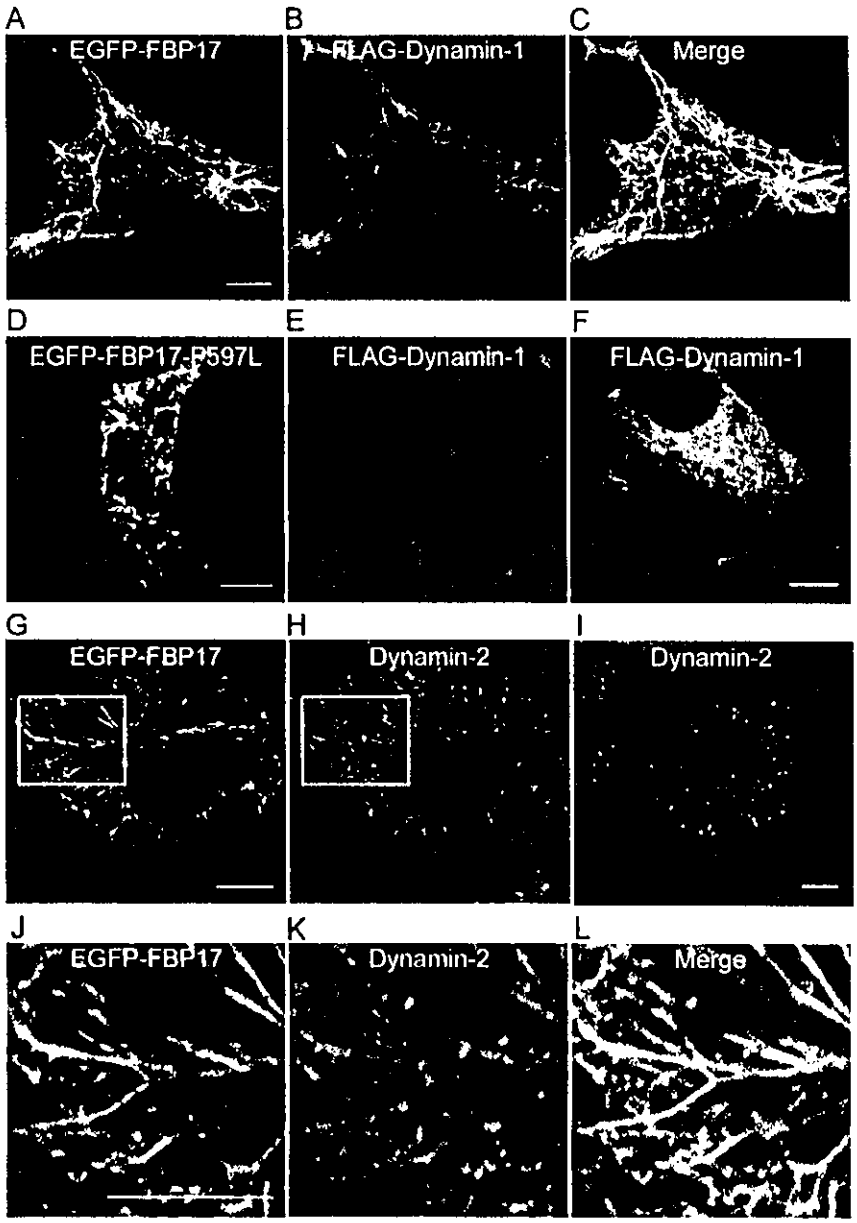

FIG. 6. **FBP17 co-localizes with dynamin in an SH3 domain-dependent manner.** *A–C*, EGFP-tagged FBP17 and FLAG-tagged dynamin-1 were coexpressed in COS-1 cells. The FBP17 image (*green*), the dynamin-1 image (FLAG-tagged dynamin-1 detected by Alexa 546; *red*), and superimposed image (*Merge*) were obtained using an Olympus BX50EI confocal microscope. *D* and *E*, EGFP-tagged FBP17-P597L and FLAG-tagged dynamin-1, respectively, were coexpressed in COS-1 cells. Cells were imaged similarly to those in *A* and *B*. *F*, COS-1 cells expressing FLAG-tagged dynamin-1 alone were imaged. Note that FBP17 but not FBP17-P597L co-localized with dynamin-1. *G* and *H*, COS-1 cells expressing EGFP-tagged FBP17 were imaged for EGFP (*green*) and for endogenous dynamin-2 detected by anti-dynamin-2 antibody followed by incubation with Alexa 546-labeled secondary antibody (*red*), respectively. *I*, endogenous dynamin-2 in parental COS-1 cells is shown. Note that endogenous dynamin-2 co-localized with the FBP17-induced tubular structure. *J–L*, the *boxed regions* in *G* and *H* were enlarged and are shown in *J* and *K*, respectively, and superimposed in *L*.

SH3 domain in its C terminus like PACSIN. EGFP-tagged full-length FBP17 was co-immunoprecipitated with FLAG-tagged dynamin-1, as was PACSIN-1 (Fig. 5*A*). To examine whether the association of FBP17 with dynamin-1 depends on the SH3 domain, we used the derivative of FBP17 with a nonfunctional SH3 domain (FBP17-SH3-P597L) and FBP17-N2 lacking the SH3 domain. As expected, EGFP-tagged full-length FBP17 and FBP17-SH3 were co-immunoprecipitated with FLAG-tagged dynamin-1 (Fig. 5*B*, *lanes 3* and *5*), whereas FBP17-N2 and FBP17-SH3-P597L were not (*lanes 4* and *6*), indicating that the association of FBP17 with dynamin-1 is dependent upon the SH3 domain of FBP17.

Dynamin-2 is ubiquitously expressed, whereas dynamin-1 is expressed exclusively in neurons, and dynamin-3 is restricted to the testis, brain, and lung (5). FBP17 is mostly expressed in the brain and testis (Fig. 2*A*). Therefore, we tested whether dynamin-2 and dynamin-3, in addition to dynamin-1, associate with FBP17 by pull-down assays using the glutathione *S*-transferase (GST)-fused SH3 domain of FBP17 (Supplemental Fig. 2*A*). EGFP-tagged dynamin-1, -2, and -3 bound to the GST-fused SH3 domain of FBP17 but not to GST alone or GST fused to the nonfunctional SH3 domain of FBP17 (FBP17-SH3-P597L). These results demonstrate that FBP17 associates with dynamin family proteins in an SH3 domain-dependent manner.

FBP17 Co-localizes with Dynamin—We proceeded to examine the co-localization of FBP17 with dynamin in COS-1 cells. EGFP-FBP17 expressed in COS-1 cells co-localized with FLAG-tagged dynamin expressed in the same cells (Fig. 6, *A–C*), whereas an SH3 mutant incapable of associating with dynamin did not co-localize with dynamin (Fig. 6, *D* and *E*). Although dynamin-1 expressed alone in COS-1 cells exhibited a diffuse staining pattern (Fig. 6*F*), dynamin-1 coexpressed with FBP17 exhibited a tubular pattern (Fig. 6*B*), indicating that dynamin-1 co-localizes with FBP17. We further examined the co-localization of FBP17 with endogenous dynamin-2 in COS-1 cells. Endogenous dynamin-2 was detected as small dots using anti-dynamin-2 antibody (Fig. 6*I*), whereas it co-localized with FBP17 in COS-1 cells expressing EGFP-FBP17 (Fig. 6, *G*, *H*, and *J–L*). These results suggest that FBP17 may be involved in endocytic signaling via dynamin.

Involvement of FBP17 in Dynamin-mediated Endocytosis—To assess the consequence of the association of FBP17 with dynamin, we compared the localization of the molecules processed in the endocytic pathways with that of FBP17.

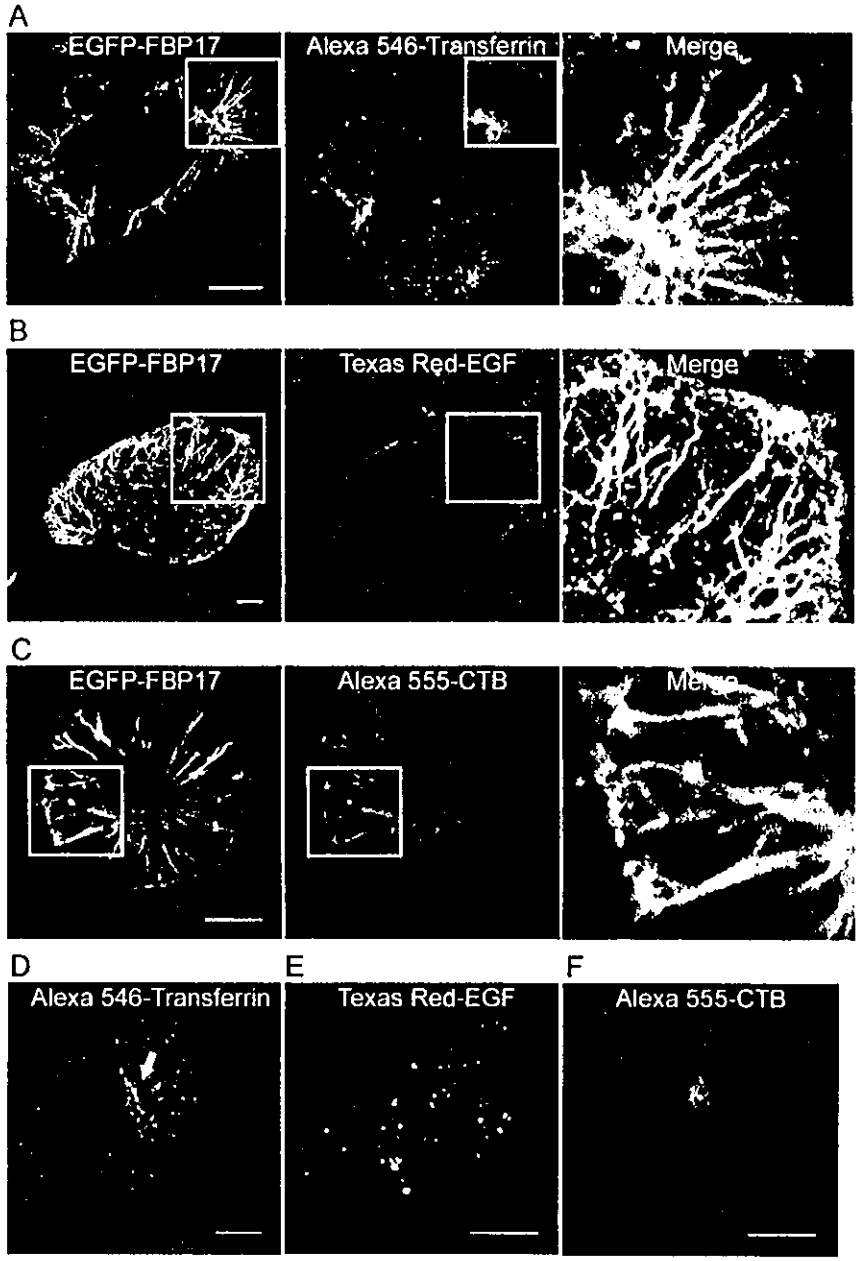

FIG. 7. **FBP17 co-localizes with transferrin, EGF, and CTB.** *A*, COS-1 cells transfected with pCA-EGFP-FBP17 for 24 h were incubated with Alexa 546-conjugated transferrin as described under "Experimental Procedures." The EGFP image (*green*) and the Alexa 546 image (*red*) were obtained using an Olympus BX50EI confocal microscope. The *boxed areas* in both the EGFP and Alexa 546 images were enlarged and are superimposed (*Merge*). *B*, COS-1 cells expressing EGFP-FBP17 were incubated with Texas Red-EGF and imaged similarly to those in *A*. *C*, COS-1 cells expressing EGFP-FBP17 were incubated with CTB and imaged similarly to those in *A*. *D–F*, parental COS-1 cells were incubated with Alexa 546-conjugated transferrin, Texas Red-EGF, and Alexa 555-conjugated CTB, respectively, for 20 min at 37 °C; fixed with 2% paraformaldehyde; and imaged though an Olympus BX50EI confocal microscope. Note that fluorescence-tagged transferrin, EGF, and CTB co-localized with the FBP17-induced tubular structure and that transferrin uptake in the cell was observed as vesicles indicated by the *arrow* in *D*. *Bars* = 10 μm.

Transferrin and EGF are endocytosed in a clathrin-dependent manner. Alexa 546-labeled transferrin was internalized along with FBP17 in COS-1 cells expressing FBP17 at 37 °C (Fig. 7*A*), whereas it was taken up as vesicles in parental COS-1 cells (Fig. 7*D*). We further examined whether the transferrin distribution follows the endocytic pathway. Whereas transferrin was observed as internalized vesicles near the nucleus at 37 °C (Fig. 7*D*), it was not when incubated at 4 °C (Fig. 8*A*). Although COS-1 cells expressing FBP17 exhibited the tubular structure, transferrin was not observed along these tubules at 4 °C (Fig. 8, *B* and *C*). These results suggest that FBP17-induced tubules involve transferrin uptake in an endocytosis-dependent manner. Similarly, Texas Red-labeled EGF was found at the tubular structure in COS-1 cells expressing FBP17, although EGF was found in a vesicular pattern in parental COS-1 cells (Fig. 7, *B* and *E*). CTB has been used as a marker for caveolae-mediated endocytosis (25). Caveolin-mediated endocytosis is dependent upon dynamin (2). We therefore examined the involvement of FBP17 in caveolin-mediated internalization of CTB in COS-1 cells expressing FBP17. Internalized CTB localized to FBP17-marked tubules, whereas CTB internalized in parental cells exhibited a vesicular pattern (Fig. 7, *C* and *F*). These data suggest that FBP17 is involved in dynamin-mediated endocytosis in both a clathrin-dependent and -independent manner.

Internalization of FBP17-induced Tubules Is Dependent upon Dynamin—Dynamin-1-K44A is a dominant-negative mutant of dynamin that is defective in GTP hydrolysis and GTP binding and therefore inhibits clathrin-dependent endocytosis and caveolin-mediated internalization (4). We used this mutant to examine the mechanism by which dynamin is involved in the internalization of FBP17-induced tubes. The FBP17-induced tubular structure was internalized (Fig. 1*D*) and co-localized with dynamin (Fig. 6). Hence, we hypothesized that dynamin-1-K44A perturbs the internalization of the tubular structure. The EGFP intensity of COS-1 cells expressing both EGFP-FBP17 and dynamin-1-K44A was compared with that of COS-1 cells expressing only EGFP-FBP17. COS-1 cells expressing both FBP17 and dynamin-1-K44A were distinguished from those expressing only EGFP-FBP17 by internal ribosomal en-

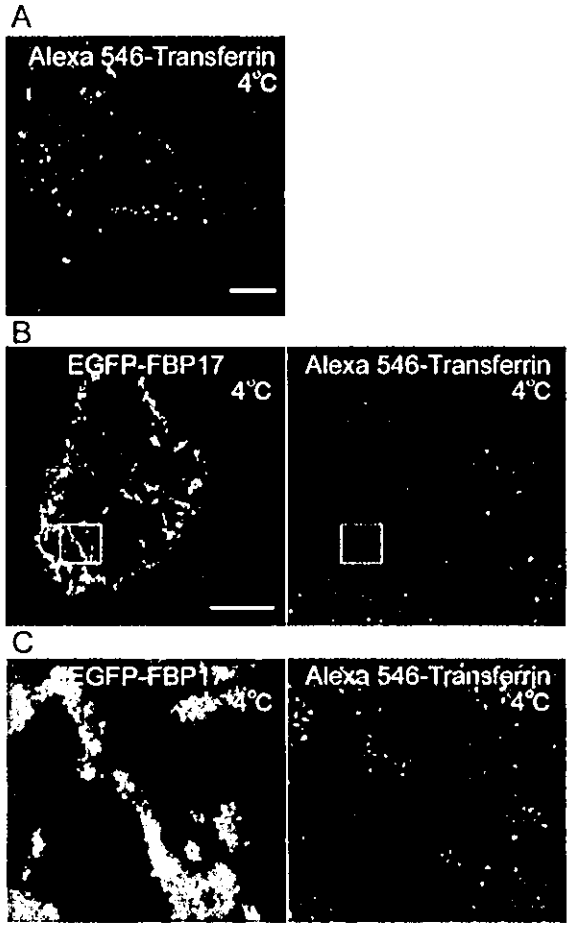

FIG. 8. **Transferrin uptake is mediated by endocytosis in COS-1 cells expressing FBP17.** COS-1 cells expressing EGFP-tagged FBP17 were incubated with Alexa 546-conjugated transferrin at 4 °C instead of 37 °C. *A*, parental COS-1 cells were incubated with Alexa 546-conjugated transferrin at 4 °C and imaged as described in the legend to Fig. 7. Note that there was no vesicular uptake of transferrin at 4 °C, in contrast to 37 °C. *Bar* = 10 μm. *B*, COS-1 cells expressing FBP17 were imaged after incubation with Alexa 546-conjugated transferrin at 4 °C. The EGFP image (*green*) and the Alexa 546 image (*red*) are shown. *Bar* = 10 μm. *C*, the *boxed area* in *B* was enlarged. Note that transferrin did not co-localize with FBP17-induced tubules.

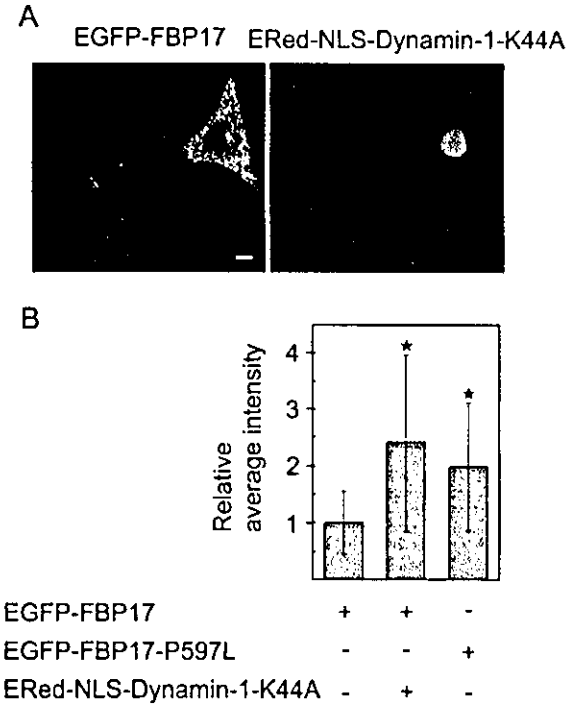

FIG. 9. **Internalization of FBP17-induced tubules depends upon dynamin.** COS-1 cells were transfected with pCA-EGFP-FBP17 and pERed-NLS-dynamin-1-K44A. COS-1 cells expressing dynamin-1-K44A were marked by internal ribosomal entry signal-driven nuclear localization signal-tagged DsRed-Express. *A*, the EGFP image (*green*) and the DsRed image (*red*) are shown. Note that the cell expressing both FBP17 and dynamin-1-K44A (*right cell*) was brighter than the cell expressing only FBP17 (*left cell*). *Bar* = 10 μm. *B*, the EGFP intensity of each of 50 cells expressing FBP17, FBP17 with dynamin-1-K44A, or FBP17-P597L was measured, and the average intensity of each group over FBP17 is indicated as relative average intensity ± S.D. Significant differences between FBP17 and FBP17 with dynamin-1-K44A and between FBP17 and FBP17-P597L by *t* test are indicated by *asterisks* ($p < 0.05$).

try signal-driven red fluorescence in the nucleus. The cells expressing both FBP17 and dynamin-1-K44A were brighter than those expressing only FBP17 (Fig. 9*A*). The quantitative results are shown in Fig. 9*B*. Consistently, cells expressing EGFP-FBP17-P597L, which were incapable of associating with dynamin but capable of inducing tubules, were brighter than those expressing wild-type FBP17 (Fig. 9*B*), suggesting the involvement of endogenous dynamin-2 present in COS-1 cells. These results indicate that the internalization of FBP17-induced tubules is mediated by dynamin.

DISCUSSION

We have demonstrated that FBP17 forms tubular invaginations when expressed in cultured cells. Although Rapostlin, a rat ortholog of human FBP17, partially localizes to microtubules when expressed in HeLa cells (15), FBP17 did not localize to any components of the cytoskeleton such as microtubules, intermediate filaments, and actin fibers (Supplementary Fig. 1). FBP17-induced tubules originated from the plasma membrane and grew toward the cytoplasm, suggesting that FBP17 is involved in endocytosis.

FBP17 associates with dynamin in an SH3 domain-dependent manner. Among dynamin-associating molecules, PACSIN/syndapin, like FBP17, has an N-terminal FCH domain and a C-terminal SH3 domain (18, 24). FBP17 containing a nonfunctional SH3 domain did not associate with dynamin, indicating that the association between FBP17 and dynamin depends on the interaction between the SH3 domain of FBP17 and the proline-rich motif of dynamin. Consistently, dynamin co-localized with the FBP17-induced tubular structure (Fig. 6). Our data are in agreement with results showing that dynamin localizes to the tubular structure formed by muscle amphiphysin-2 (M-amphiphysin-2) (26).

FBP17-induced tubular invagination is strongly reminiscent of that generated by an isoform of amphiphysin, M-amphiphysin-2. GFP-tagged M-amphiphysin-2 induces massive tubulation in Chinese hamster ovary cells (26). There are common characteristics between M-amphiphysin-2 and FBP17. First, it is noteworthy that the SH3 domain in the C termini of both M-amphiphysin-2 and FBP17 are dispensable for tubulation (Fig. 4*C*). The BAR domain (Bin1/amphiphysin/Rvs) of M-amphiphysin-2 is probably responsible for membrane targeting via membrane phosphatidylinositol 4,5-phosphates and tubule formation (26–28). Thus, the FCH domain of FBP17, like the BAR domain, may function as a membrane-targeting domain and also a plasma membrane-deforming domain. Second, the N termini of amphiphysin-2 and FBP17 are also essential for dimerization (29). We found that the N terminus of FBP17 consisting of the FCH domain, a coiled-coil domain, and a proline-rich region was required for self-assembly to form tubular structures. Third, both FBP17 and M-amphiphysin-2 co-localize with dynamin in cultured cells. These results

prompted us to examine the involvement of FBP17 in endocytosis since amphiphysin participates in endocytosis.

The various SH3 domain-binding partners of dynamin affect vesiculation differently during endocytosis, which depends upon the pinch-off effect of dynamin when it hydrolyzes GTP (3, 30). We have demonstrated that FBP17 associated and colocalized with dynamin and that FBP17 involved dynamin-mediated transferrin and EGF endocytosis (Fig. 7). In addition, the internalization of FBP17-induced tubules was regulated by dynamin (Fig. 9). These results are consistent with the observation that amphiphysin-dynamin interaction enhances dynamin-mediated endocytosis in a clathrin-dependent manner (28). In contrast, all PACSIN isoforms block clathrin-mediated transferrin endocytosis (18), and endophilin perturbs dynamin-mediated vesiculation (31). Thus, dynamin-binding proteins such as syndapin, amphiphysin-2, endophilin, and intersectin appear to be involved at distinct stages of clathrin-mediated vesicle formation (32). Accordingly, FBP17 may participate in the recruitment of dynamin, and the recruited dynamin may then pinch off the tubules or vesicles induced by FBP17 *in vivo*.

Given that FBP17 was expressed in the testis (Fig. 2) and that dynamin-2 and dynamin-3 are expressed in the testis (7), the association of FBP17 with dynamins in the testis is likely to be involved in spermatogenesis. The expression of Rnd2, which belongs to the Rho family of GTPases and is an RBD partner of Rapostlin, an ortholog of FBP17, is restricted to germ cells at the spermatocyte and spermatid stages (33, 34). The expression of FBP17 determined by immunohistochemistry paralleled Rnd2 expression in germ cells. Hence, the Rnd2-FBP17-dynamin complex may be involved in endocytosis required for sperm maturation in the testis. In conclusion, we have demonstrated that FBP17 forms membrane invaginations originating from the plasma membrane and that FBP17 is likely to be involved in dynamin-dependent endocytosis.

Acknowledgments—We thank Drs. Y. Nishimune and K. Kashima for advice; H. K. Surks and J. T. Pearson for critical reading of the manuscript; and M. Sone, Y. Ohba, N. Irisawa, and M. Sato for technical assistance.

REFERENCES

1. Nobes, C. D., and Hall, A. (1995) *Cell* **81,** 53–62
2. Conner, S. D., and Schmid, S. L. (2003) *Nature* **422,** 37–44
3. Sweitzer, S. M., and Hinshaw, J. E. (1998) *Cell* **93,** 1021–1029
4. Hinshaw, J. E. (2000) *Annu. Rev. Cell Dev. Biol.* **16,** 483–519
5. Cao, H., Garcia, F., and McNiven, M. A. (1998) *Mol. Biol. Cell* **9,** 2595–2609
6. Sontag, J. M., Fykse, E. M., Ushkaryov, Y., Liu, J. P., Robinson, P. J., and Sudhof, T. C. (1994) *J. Biol. Chem.* **269,** 4547–4554
7. Kamitani, A., Yamada, H., Kinuta, M., Watanabe, M., Li, S. A., Matsukawa, T., McNiven, M., Kumon, H., and Takei, K. (2002) *Biochem. Biophys. Res. Commun.* **294,** 261–267
8. Nabi, I. R., and Le, P. U. (2003) *J. Cell Biol.* **161,** 673–677
9. Pelkmans, L., and Helenius, A. (2002) *Traffic* **3,** 311–320
10. Schmid, S. L., McNiven, M. A., and De Camilli, P. (1998) *Curr. Opin. Cell Biol.* **10,** 504–512
11. Slepnev, V. I., and De Camilli, P. (2000) *Nat. Rev. Neurosci.* **1,** 161–172
12. Chan, D. C., Bedford, M. T., and Leder, P. (1996) *EMBO J.* **15,** 1045–1054
13. Fuchs, U., Rehkamp, G., Haas, O. A., Slany, R., Konig, M., Bojesen, S., Bohle, R. M., Damm-Welk, C., Ludwig, W. D., Harbott, J., and Borkhardt, A. (2001) *Proc. Natl. Acad. Sci. U. S. A.* **98,** 8756–8761
14. Tian, L., Nelson, D. L., and Stewart, D. M. (2000) *J. Biol. Chem.* **275,** 7854–7861
15. Fujita, H., Katoh, H., Ishikawa, Y., Mori, K., and Negishi, M. (2002) *J. Biol. Chem.* **277,** 45428–45434
16. Greer, P. (2002) *Nat. Rev. Mol. Cell. Biol.* **3,** 278–289
17. Kogata, N., Masuda, M., Kamioka, Y., Yamagishi, A., Endo, A., Okada, M., and Mochizuki, N. (2003) *Mol. Biol. Cell* **14,** 3553–3564
18. Modregger, J., Ritter, B., Witter, B., Paulsson, M., and Plomann, M. (2000) *J. Cell Sci.* **113,** 4511–4521
19. Yoshizaki, H., Ohba, Y., Kurokawa, K., Itoh, R. E., Nakamura, T., Mochizuki, N., Nagashima, K., and Matsuda, M. (2003) *J. Cell Biol.* **162,** 223–232
20. Ohnishi, J., Ohnishi, E., Jin, M., Hirano, W., Nakaae, D., Matsui, H., Kimura, A., Sawa, H., Nakayama, K., Shibuya, H., Nagashima, K., and Takahashi, T. (2001) *Mol. Endocrinol.* **15,** 747–764
21. Nagashima, K., Endo, A., Ogita, H., Kawana, A., Yamagishi, A., Kitabatake, A., Matsuda, M., and Mochizuki, N. (2002) *Mol. Biol. Cell* **13,** 4231–4242
22. Mukherjee, S., and Maxfield, F. R. (2000) *Traffic* **1,** 203–211
23. Wasiak, S., Quinn, C. C., Ritter, B., de Heuvel, E., Baranes, D., Plomann, M., and McPherson, P. S. (2001) *J. Biol. Chem.* **276,** 26622–26628
24. Qualmann, B., and Kelly, R. B. (2000) *J. Cell Biol.* **148,** 1047–1062
25. Parton, R. G., and Richards, A. A. (2003) *Traffic* **4,** 724–738
26. Lee, E., Marcucci, M., Daniell, L., Pypaert, M., Weisz, O. A., Ochoa, G. C., Farsad, K., Wenk, M. R., and De Camilli, P. (2002) *Science* **297,** 1193–1196
27. Zhang, B., and Zelhof, A. C. (2002) *Traffic* **3,** 452–460
28. Takei, K., Slepnev, V. I., Haucke, V., and De Camilli, P. (1999) *Nat. Cell Biol.* **1,** 33–39
29. Ramjaun, A. R., Philie, J., de Heuvel, E., and McPherson, P. S. (1999) *J. Biol. Chem.* **274,** 19785–19791
30. Sever, S., Damke, H., and Schmid, S. L. (2000) *J. Cell Biol.* **150,** 1137–1148
31. Farsad, K., Ringstad, N., Takei, K., Floyd, S. R., Rose, K., and De Camilli, P. (2001) *J. Cell Biol.* **155,** 193–200
32. Simpson, F., Hussain, N. K., Qualmann, B., Kelly, R. B., Kay, B. K., McPherson, P. S., and Schmid, S. L. (1999) *Nat. Cell Biol.* **1,** 119–124
33. Nobes, C. D., Lauritzen, I., Mattei, M. G., Paris, S., Hall, A., and Chardin, P. (1998) *J. Cell Biol.* **141,** 187–197
34. Naud, N., Toure, A., Liu, J., Pineau, C., Morin, L., Durseuil, O., Escalier, D., Chardin, P., and Gacon, G. (2003) *Biochem. J.* **372,** 105–112

THE JOURNAL OF BIOLOGICAL CHEMISTRY
Vol. 279, No. 43, Issue of October 22, pp. 44756–44762, 2004
Printed in U.S.A.

Cell Type-specific Regulation of RhoA Activity during Cytokinesis*[S]

Received for publication, March 1, 2004, and in revised form, August 2, 2004
Published, JBC Papers in Press, August 12, 2004, DOI 10.1074/jbc.M402292200

Hisayoshi Yoshizaki‡§, Yusuke Ohba‡, Maria-Carla Parrini‡¶, Natalya G. Dulyaninova‖, Anne R. Bresnick‖, Naoki Mochizuki§, and Michiyuki Matsuda‡**

From the ‡Department of Tumor Virology, Research Institute for Microbial Diseases, Osaka University, Yamadaoka, Suita-shi, Osaka 565-0871, the §Department of Structural Analysis, National Cardiovascular Center Research Institute, Fujishirodai, Suita-shi, Osaka 565-8565, Japan, and the ‖Department of Biochemistry, Albert Einstein College of Medicine, Bronx, New York 10461

Rho family GTPases play pivotal roles in cytokinesis. By using probes based on the principle of fluorescence resonance energy transfer (FRET), we have shown that in HeLa cells RhoA activity increases with the progression of cytokinesis. Here we show that in Rat1A cells RhoA activity remained suppressed during most of the cytokinesis. Consistent with this observation, the expression of C3 toxin inhibited cytokinesis in HeLa cells but not in Rat1A cells. Furthermore, the expression of a dominant negative mutant of Ect2, a Rho GEF, or Y-27632, an inhibitor of the Rho-dependent kinase ROCK, inhibited cytokinesis in HeLa cells but not in Rat1A cells. In contrast to the activity of RhoA, the activity of Rac1 was suppressed during cytokinesis and started increasing at the plasma membrane of polar sides before the abscission of the daughter cells in both HeLa and Rat1A cells. This type of Rac1 suppression was shown to be essential for cytokinesis because a constitutively active mutant of Rac1 induced a multinucleated phenotype in both HeLa and Rat1A cells. Moreover, the involvement of MgcRacGAP/CYK-4 in this suppression of Rac1 during cytokinesis was shown by the use of a dominant negative mutant. Because ML-7, an inhibitor of myosin light chain kinase, delayed the cytokinesis of Rat1A cells and because Pak, a Rac1 effector, is known to suppress myosin light chain kinase, the suppression of the Rac1-Pak pathway by MgcRacGAP may play a pivotal role in the cytokinesis of Rat1A cells.

After chromosomal separation at the onset of anaphase, cytokinesis creates two daughter cells endowed with a complete set of chromosomes and cytoplasmic organelles. During this period, cortical actin and myosin II begin to move toward the equatorial region, where they form a contractile cleavage furrow (1–3). Rho family GTPases, which regulate a number of cell functions including gene expression and cell adhesion (4), also play a pivotal role in cytokinesis (2, 5, 6). Among them, RhoA has been shown to be necessary for cytokinesis in a variety of cell types including *Xenopus* and sand dollar eggs (7). Furthermore (8, 9), significant progress has been made in the identification of RhoA effectors during cytokinesis (5). One RhoA effector, Rho kinase/ROCK, stimulates myosin II regulatory light chain (MLC)[1] directly by phosphorylation and indirectly by the inhibition of myosin phosphatase (10, 11). Another RhoA effector, citron kinase, also phosphorylates and activates MLC (12). This phosphorylation of MLC is believed to lead to actomyosin contractility and thereby to cytokinesis. However, the role of RhoA in cytokinesis may not be identical in adherent cells and in eggs or poorly adherent cells; well adherent NRK and Swiss 3T3 cells undergo cell division in the presence of an inhibitor of Rho, C3 ribosyltransferase, suggesting that cytokinesis may proceed by a RhoA-independent mechanism in some cell types (13).

In addition to RhoA, Rac1, and Cdc42 have also been implicated in the cytokinesis of mammalian cells, based on the appearance of multinucleated cells among cells expressing constitutively active Rac1 or Cdc42 (14, 15). In agreement with this view, it has been speculated that low microtubule density at the equatorial region leads to the suppression of Rac1 (6). This suppression of Rac1 activity down-regulates Pak, a kinase known to phosphorylate and thereby suppress MLCK (16). Therefore, the suppression of Rac1 may also be involved in the contraction of the cleavage furrow.

The activity of Rho family GTPases is regulated by the balance between guanine nucleotide exchange factors (GEFs) and GTPase-activating proteins (GAPs); GEF activates Rho by catalyzing the uptake of GTP, whereas GAP stimulates the GTPase activity of Rho, leading to its inactivation. Molecular and genetic studies have shown that a mammalian Rho GEF, ECT2, and its *Drosophila melanogaster* ortholog, Pebble (PBL), are required for cytokinesis (17, 18). Recent studies have shown that these GEFs may be particularly important in the determination of the place and timing of cytokinesis (19, 20). In addition to the GEFs, GAPs also appear to play a critical role during cytokinesis. A GAP for the Rho family GTPases, MgcRacGAP/CYK-4, is a component of the central spindlin complex, which bundles microtubules in the central spindle (20–23). The inhibition of MgcRacGAP/CYK-4 by mutants or RNA interference inhibits cytokinesis, inducing multinucle-

* This work was supported in part by a grant for scientific research on priority areas (special) from the Ministry of Education, Science, Sports, and Culture of Japan and by a grant for comprehensive research on aging and health from the Ministry of Health, Labor, and Welfare. The costs of publication of this article were defrayed in part by the payment of page charges. This article must therefore be hereby marked "*advertisement*" in accordance with 18 U.S.C. Section 1734 solely to indicate this fact.

[S] The on-line version of this article (available at http://www.jbc.org) contains a figure.

¶ Fellow supported by the Japan Society for the Promotion of Science.

** To whom correspondence should be addressed: Dept. of Tumor Virology, Research Institute for Microbial Diseases, Osaka University, Yamadaoka, Suita-shi, Osaka 565-0871, Japan. Tel.: 81-6-6879-8316; Fax: 81-6-6879-8314; E-mail: matsudam@biken.osaka-u.ac.jp.

[1] The abbreviations used are: MLC, myosin II regulatory light chain; GEF, guanine nucleotide exchange factor; GAP, GTPase-activating protein; FRET, fluorescence resonance energy transfer; BrdUrd, bromo-2′-deoxyuridine; MLCK, myosin light chain kinase; NRK, normal rat kidney; GFP, green fluorescent protein; YFP, yellow fluorescent protein; CFP, cyan fluorescent protein; DMEM, Dulbecco's modified Eagle's medium; FBS, fetal bovine serum; PBS, phosphate-buffered saline; DIC, differential interference contrast.

ated cells (22, 23). MgcRacGAP/CYK-4 is 20–30-fold more active toward Rac1 and Cdc42 than toward RhoA (21), but becomes active toward RhoA upon phosphorylation by Aurora B (24). This MgcRacGAP/CYK-4-mediated RhoA suppression has been shown to be required for proper cortical activity during cytokinesis (25). Furthermore, PRC1, a human spindle-associated cyclin-dependent kinase substrate, binds to and inhibits the Cdc42 GAP activity of MgcRacGAP/CYK-4 (26). Therefore, at least three Rho family GTPases, RhoA, Rac1, and Cdc42, can function as potential targets of MgcRacGAP/CYK-4 during cytokinesis.

Because the precise spatio-temporal regulation of the Rho family GTPases is critical for the progression of cytokinesis, it is necessary to visualize changes in the activity of these GTPases in living cells. To this end, we developed probes for the Rho family GTPases based on the principle of fluorescent resonance energy transfer (FRET) (27, 28). By using these FRET-based probes, we have shown that the activities of RhoA, Rac1, and Cdc42 decrease upon entry into mitosis in HeLa cells (28). Although RhoA activity starts to increase after the initiation of cytokinesis, the activities of Rac1 and Cdc42 begin to increase at approximately the time of the abscission of daughter cells. Here we extended our previous study by using Rat1A cells in place of HeLa cells, and we demonstrated that RhoA activation at the onset of cytokinesis is not found in this cell type. In accord with this observation, the cytokinesis of Rat1A was not inhibited by inhibitors of RhoA. These observations indicate that the activation of and the requirement for RhoA during cytokinesis are cell type-specific.

EXPERIMENTAL PROCEDURES

FRET Probes, Plasmids, and Recombinant Adenoviruses—The FRET probes, designated as Raichu-Rac1 and Raichu-RhoA, have been described previously (27, 28). The cDNAs for Rac1-V12 and Rac1-N17 were expressed from a pIRM21-FLAG expression vector containing a FLAG tag and an internal ribosomal entry site followed by the cDNA of a red fluorescent protein, dsFP593, at the 5′- and 3′-side of the cloning site, respectively (27). An expression vector of a dominant negative form of Ect2, Ect2-N, was obtained from T. Miki (National Institutes of Health). A dominant negative mutant of MgcRacGAP was obtained from T. Kitamura (Institute for Medical Sciences, University of Tokyo) and was subcloned into pERedMit, which, at the 3′-side of the cloning site, contained an internal ribosomal entry site followed by the cDNA of Express Red (BD Biosciences) fused to mitochondria-targeting signal. cDNA of Pak T423E mutant was obtained from G. M. Bokoch (The Scripps Research Institute) (29) and subcloned into pERedNES, which contained an internal ribosomal entry site followed by the cDNA of Express Red fused to the nuclear export signal. Use of these two marker proteins with different targeting signals allows us to identify cells that express both of the expression plasmids. A recombinant adenovirus carrying C3 toxin cDNA, adeno-GFP-C3, and a control virus carrying GFP alone were obtained from H. Kurose (Kyusyu University, Fukuoka, Japan).

Cells—HeLa and NIH3T3 cells were purchased from the Human Science Research Resources Bank (Sennan-shi, Japan) and from the RIKEN Gene Bank (Wako-shi, Japan), respectively. Rat1A and NRK cells were gifts from Y. Nakabeppu (Kyushu University, Fukuoka, Japan) and H. Okayama (University of Tokyo, Tokyo, Japan), respectively. HeLa, NIH3T3, and Rat1A cells were maintained in DMEM (Sigma) supplemented with 10% FBS. NRK cells were maintained in DMEM supplemented with 5% FBS. Before cell imaging, DMEM was replaced with phenol red-free minimum Eagle's medium (Nissui, Tokyo, Japan) containing 10% FBS.

FRET Imaging of Rho Family GTPases in Living Cells—FRET imaging was performed essentially as described previously (28). Briefly, cells plated on a collagen-coated 35-mm diameter glass-base dishes (Asahi Techno Glass Co., Tokyo, Japan) were transfected with Raichu expression vectors and imaged every 2 min on an Olympus IX70 inverted microscope (Olympus Optical Co., Tokyo, Japan) that was equipped with a cooled CCD camera, CoolSNAP HQ (Roper Scientific, Trenton, NJ), and controlled by MetaMorph software (Universal Imaging, West Chester, PA) (30). For dual-emission ratio imaging of the Raichu probes, we used a 440AF21 excitation filter, a 455DRLP dichroic mirror, and two emission filters, 480AF30 for CFP and 535AF26 for YFP (Omega Optical Inc., Brattleboro, VT). Cells were illuminated with a 75-watt xenon lamp through a 12% ND filter (Olympus Optical) and a 100× oil immersion objective lens. The exposure time was 0.5 s when the binning of the CCD camera was set to 4 × 4. After background subtraction, the ratio image of YFP/CFP was created with MetaMorph software and was used to represent the efficiency of the FRET.

Roles of Rho Family GTPases in Cytokinesis—Cells were infected with recombinant adenoviruses carrying GFP or GFP-C3. Thirty six hours later, the cells were labeled with BrdUrd (Sigma) for 12 h. After fixation with 70% ethanol, the cells were permeabilized with 0.1% Tween 20, followed by incubation in PBS containing 30 μg/ml DNase I (Roche Diagnostics) for 1 h. BrdUrd incorporated into the nucleus was detected with anti-BrdUrd antibody (BD Biosciences), followed by Alexa 546-conjugated anti-mouse IgG antibody (Molecular Probes, Inc., Eugene, OR). More than 100 cells that were positive for both BrdUrd and GFP were analyzed to identify the multinucleated phenotype. In other experiments, the cells were transfected with pIRM21-derived expression plasmids of Rho family GTPases or pERed-derived expression plasmids, and 48 h later, the cells expressing marker proteins were analyzed to identify the multinucleated phenotype.

Microinjection of C3 Toxin—The cDNA of C3 toxin was inserted into pGEX-6P (Amersham Biosciences). The purification of C3 was performed according to the manufacturer's protocol. Briefly, glutathione *S*-transferase-fused C3 was purified on a glutathione-Sepharose column from the cell lysates of *Escherichia coli* expressing pGEX-6P-C3. C3 was excised from glutathione *S*-transferase with PreScission protease, followed by dialysis against PBS. Cells in the metaphase were microinjected with 0.1 mg/ml C3 in PBS or with PBS alone and were analyzed to identify the multinucleated phenotype as described previously (13).

Effect of Kinase Inhibitors on Cytokinesis—Cells were treated with 40 μM Y-27632 (Calbiochem) for 4 h, 40 μM ML-7 (Calbiochem) for 5 min, or 100 μM blebbistatin (Toronto Research Chemicals Inc., North York, Ontario, Canada) for 1 min. Then, in the continuing presence of the inhibitors, cells in metaphase were identified, and such cells were recorded by DIC images created every 30 s in the case of the Rat1a cells and every 1 min in the case of the HeLa cells. By using these DIC images, the diameter of the contractile ring was measured and plotted to obtain the time course. Each time course was fitted to an exponential curve with GraFit software (Erithacus Software Ltd., Horley, UK), by which the maximum velocity and the half-time ($\tau_{1/2}$) of cleavage furrow contraction were calculated.

RESULTS AND DISCUSSION

Changes in the Activity of RhoA and Rac1 in Rat1A Cells Progressing from the G_2 to the G_1 Phase—To examine whether the changes in the activity of RhoA and Rac1 described in HeLa cells could be generalized to other cell types, we monitored spatio-temporal changes in the activities of RhoA and Rac1 by using Rat1A cells progressing from the G_2 to the G_1 phase, as described previously (28). Briefly, Rat1A cells expressing Raichu-RhoA or Raichu-Rac1 were excited at 440 nm and imaged for CFP and YFP at 475 and 530 nm, respectively. The intensity ratio YFP/CFP was used to represent the FRET efficiency of the probes, which reflects the GTP/GDP ratio on each probe. Because Raichu probes are regulated in a manner similar to that of authentic GTPases, the FRET value at each pixel of the digital image reflects the activity of the corresponding GTPase (28). Images of differential interference contrast and YFP-tagged actin were also obtained to follow the morphological changes.

At prophase, the activities of RhoA and Rac1 started decreasing, reaching a nadir at telophase, and gradually increased upon exit from the M phase (Fig. 1*A*). The activities were then averaged for the entire region of each Rat1A cell and compared with those of HeLa cells (Fig. 1*B*). RhoA activity started increasing at late telophase in Rat1A cells, whereas it did so in anaphase in the HeLa cells. The time course of the change in the activity of Rac1 was very similar between Rat1A cells and HeLa cells. In order to follow changes in activity over a long period of ~16 h, the objective lens was focused on the basal plasma membrane before imaging and was fixed during the

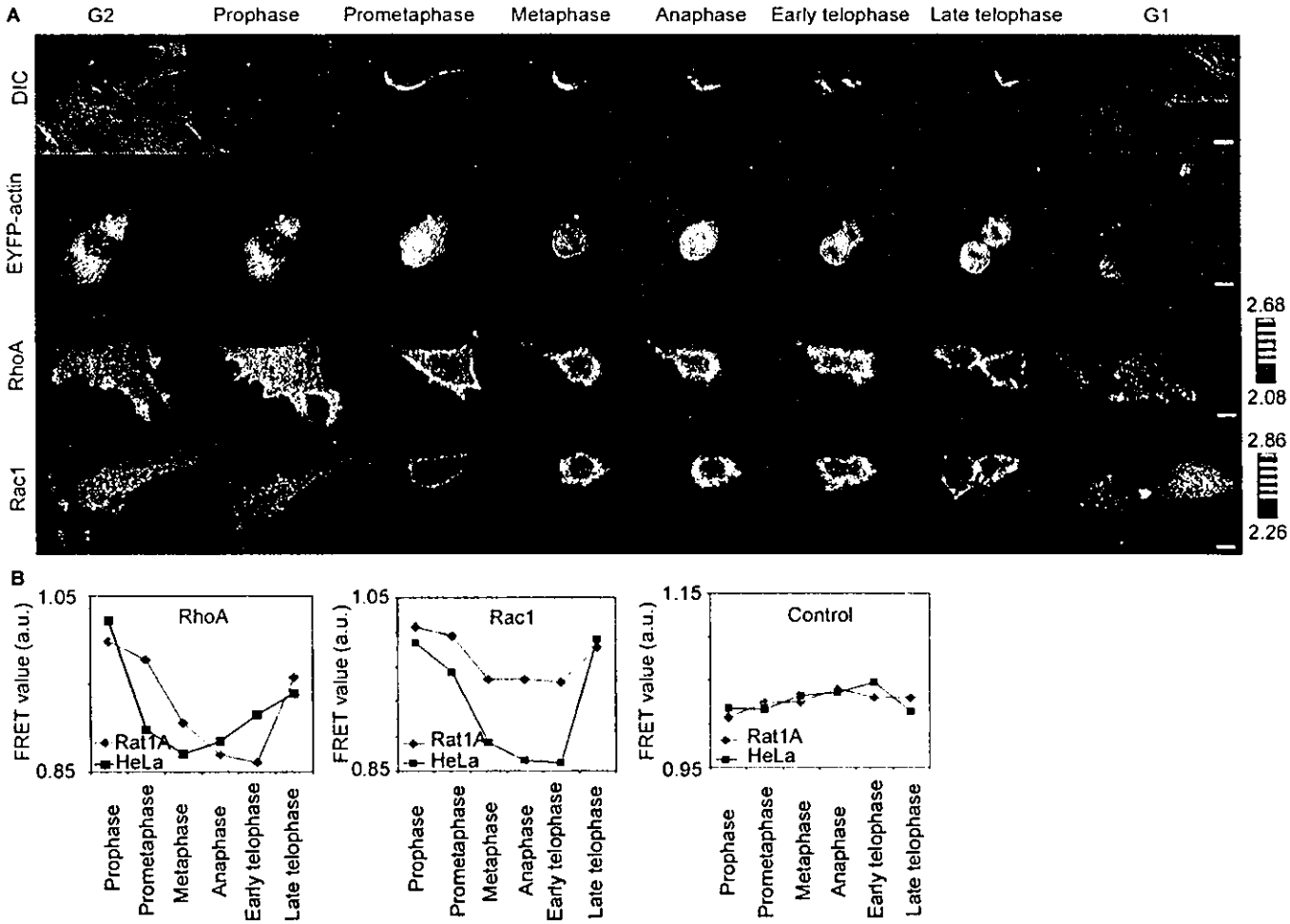

FIG. 1. **The activity of Rho family GTPases in HeLa cells progressing from the G_2 to the G_1 phase.** *A*, Rat1A cells were infected with recombinant adenoviruses for the expression of Raichu-RhoA and Raichu-Rac1, as indicated at *left*. CFP, YFP, and DIC images were obtained every 1 min with a time-lapse epifluorescent microscope. A ratio image of YFP/CFP was used to represent the FRET efficiency. The stages of the cell cycle were determined by the DIC images. Representative FRET images are shown at each stage of the cell cycle denoted at the *top* of the figure. The upper and lower limits of the ratio range are shown at the *right* of each panel. At least four similar images were obtained for each probe, and a representative image is used here. *B*, in the Rat1A cells from the images in *A*, the net intensities of YFP and CFP in each cell were measured in order to calculate the averaged YFP/CFP emission ratio. The HeLa cell experiments were performed in essentially the same manner as the Rat1A cell experiments. Because the basal level of the emission ratio varies from cell to cell, the relative emission ratio to that of the G_2 phase is used as an arbitrary unit (*a.u.*). As a control, we used Raichu-Pak-Rho as described (28).

entire experiment. Thus, upon the rounding of the cells during mitosis, the images always became out of focus. To obtain clearer images, we looked for cells that had entered into mitosis, and we acquired their images by continuously focusing the lens at the middle depth of the cells (Fig. 2*A*). The progression of cytokinesis was followed by measuring the breadth of the cells at the cleavage furrow. The averaged RhoA activity increased, whereas the constriction proceeded in HeLa cells, and in Rat1A cells, RhoA activity reached a nadir in the late phase of cytokinesis, slightly before the appearance of the mitotic midbody. We performed similar experiments with NRK and NIH3T3 cells and found that NRK cells behaved in a manner similar to that of HeLa cells, whereas NIH3T3 cells behaved in a manner similar to that of Rat1A cells (Fig. 2*B*). These observations suggest that the role of RhoA in cytokinesis is cell type-specific.

The changes in the activity of Rac1 were indistinguishable among HeLa, Rat1A, NRK, and NIH3T3 cells (Fig. 3). Suppression of Rac1 activity was most prominent at the cleavage furrow, and the increase in activity was initiated at the polar ends of the plasma membrane in both cell types.

Inhibition of Cytokinesis of HeLa and NRK Cells but Not of Rat1A and NIH3T3 Cells by C3—The lack of increase in RhoA activity during cytokinesis suggested its dispensability in the cytokinesis of Rat1A cells and NIH3T3 cells. To address this issue, we examined the effect of C3 toxin on cytokinesis. The effectiveness of C3 toxin delivered by a recombinant adenovirus was first confirmed by the loss of actin stress fibers in both HeLa and Rat1A cells.[2] To exclude cells that were G_1-arrested by the inactivation of Rho family GTPases (31), we stained the cells with BrdUrd, and we determined the number of multinucleated cells among those positive for both BrdUrd and GFP (Fig. 4*A*). The expression of GFP-C3 significantly induced the multinucleated phenotype in more than 50% of the HeLa cells but only in 10% of the Rat1A cells and 18% of the NIH3T3 cells. We could not perform a similar experiment by using NRK cells because of the toxicity of the recombinant adenovirus carrying GFP-C3 to this cell type. Therefore, we examined the effect of C3 by microinjecting purified C3 toxin into the cytoplasm at metaphase (Fig. 4*B*). Cytokinesis was remarkably inhibited in HeLa and NRK cells and was slightly disturbed in Rat1A cells by this manipulation. These results suggest that the requirement of RhoA for cytokinesis was less flexible in

[2] H. Yoshizaki and M. Matsuda, unpublished results.

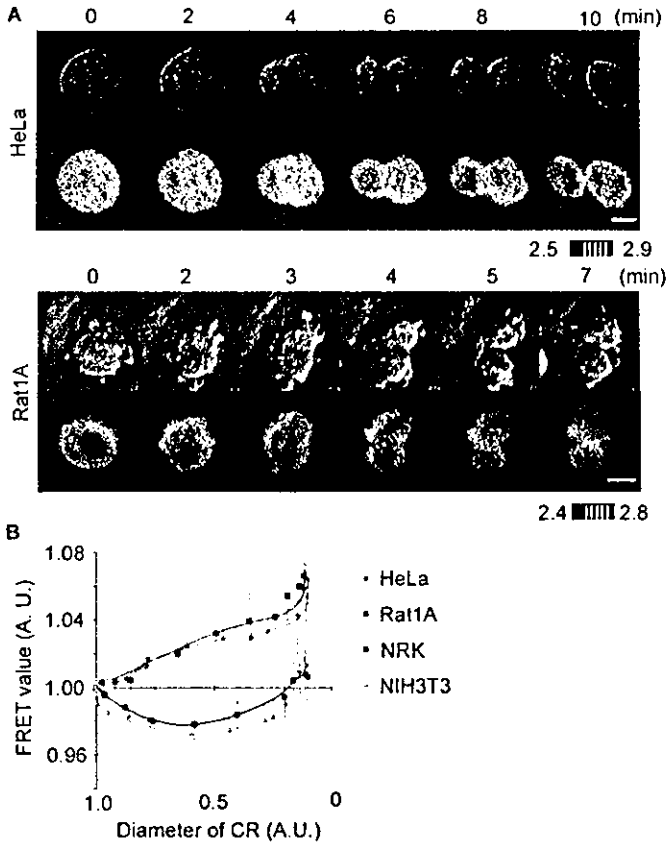

FIG. 2. **Changes in the activity of RhoA during cytokinesis.** *A*, HeLa cells or Rat1A cells expressing Raichu-RhoA were photographed as in Fig. 1*A*, except that the fluorescent images were focused on the contour of the cells and subjected to median filtering in order to reduce noise. The elapsed time and the phases are denoted at the *top* of the figure. Time zero is set to metaphase. *B*, the net intensities of YFP and CFP in each cell were measured in order to calculate the average emission ratio. The progression of cytokinesis was monitored by a decrease in the diameter of the contractile ring (*CR*). The *abscissa* shows the diameter of contractile ring in arbitrary units (*A.U.*), the value of which varies from 1 at the initiation to 0 at the end of cytokinesis. NRK cells and NIH3T3 cells expressing Raichu-RhoA were imaged, and the emission ratio (YFP/CFP) was obtained as in *A*. *Bars* indicate *error bars* from five cells.

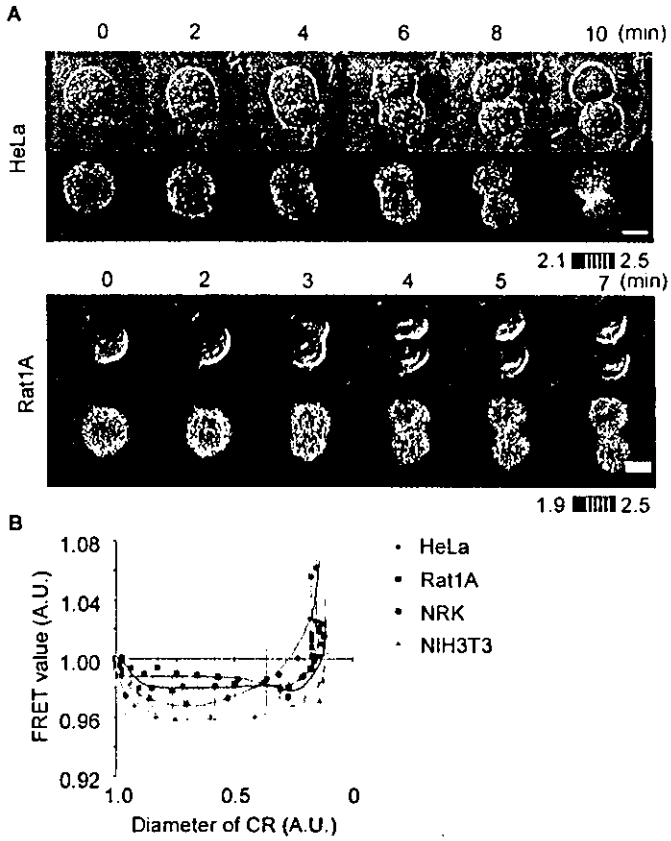

FIG. 3. **Changes in the activity of Rac1 during cytokinesis.** *A*, HeLa cells or Rat1A cells expressing Raichu-Rac1 were photographed as in Fig. 1*A*, except that the fluorescent images were focused on the contour of the cells and subjected to median filtering in order to reduce noise. The elapsed time and the phases are denoted at the *top* of the figure. The time 0 is set to metaphase. *B*, the net intensities of YFP and CFP in each cell were measured in order to calculate the averaged emission ratio. The progression of cytokinesis was analyzed as described in Fig. 2*B*. *A.U.*, arbitrary units.

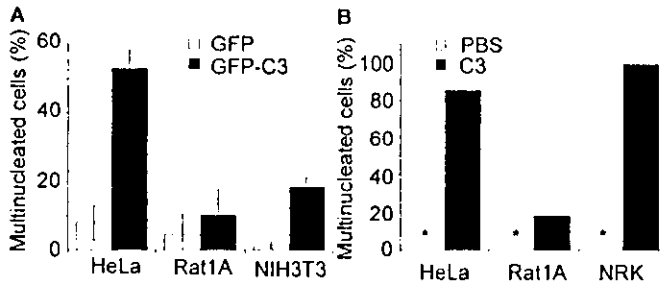

FIG. 4. **Cell type-dependent requirement of RhoA for cytokinesis.** *A*, HeLa cells, NIH3T3 cells, and Rat1A cells were infected with recombinant adenoviruses encoding GFP-C3 or GFP. Twenty four hours after infection, the cells were labeled with bromodeoxyuridine. Forty eight hours after adenovirus infection, more than 100 cells that were positive for both bromodeoxyuridine and GFP were analyzed to identify the multinucleated phenotype. Independent experiments were performed four times for HeLa and Rat1A cells and twice for NIH3T3 cells. Averaged data are shown with S.D. *B*, cells at metaphase were microinjected with C3 or PBS and were examined for the multinucleated phenotype. Fifteen cells were counted in every microinjected group. *Asterisks* indicate that no multinucleated cells were observed under that condition.

HeLa and NRK cells than in Rat1A cells and NIH3T3 cells. O'Connell *et al.* (13) have shown that the microinjection of C3 inhibits cytokinesis in HeLa cells but not in NRK cells and Swiss 3T3 cells. The discrepancy regarding the effects on NRK cells may have been due to the difference in the origin of NRK cells, the culturing conditions, or the concentration of C3. In any case, the effect of C3 on cytokinesis appeared to be dependent on the cellular context.

Role of the Suppression of Rac1 Activity in Cytokinesis—Next, we addressed the role of the suppression of Rac1 during cytokinesis. To this end, we expressed constitutively active or dominant negative mutants of Rac1 (Fig. 5*A*). The expression of Rac1-G12V significantly increased the number of multinucleated cells in both HeLa and Rat1A cells. This observation agreed with the results of previous reports, *i.e.* it was found that constitutively active Rac1 induced multinucleated cells in HeLa and porcine aortic endothelial cells (14, 15). In contrast to the constitutively active mutant, Rac1-T17N did not increase the number of multinucleated cells to a detectable level. This observation again agreed with those of previous reports (2, 21) showing that a loss of the function of Rac1 did not inhibit cytokinesis.

Among many effector molecules of Rac1, Pak may be involved in the regulation of cytokinesis. Microinjection of Pak inhibits cleavage furrow ingression of *Xenopus* egg (32). Pak phosphorylates and thereby inhibits MLCK (16, 33), which is known to promote cytokinesis through phosphorylation of myosin II (34). We found that expression of a constitutively active Pak1 mutant, Pak-T423E, significantly increased the number of multinucleated cells both in HeLa and NIH3T3 cells (Fig.

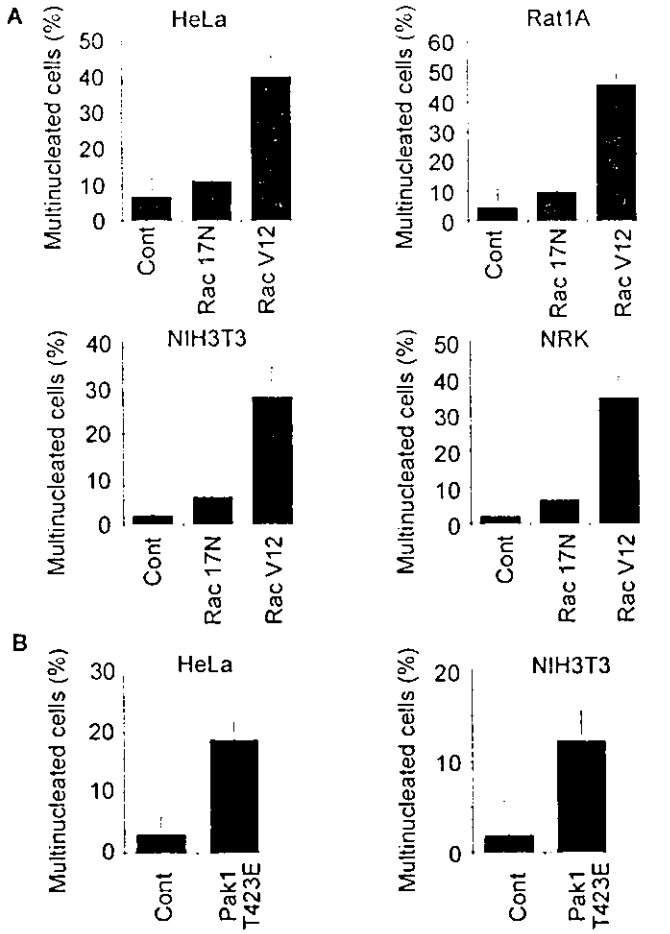

FIG. 5. **Role of Rac1 and Pak1 on cytokinesis.** *A*, HeLa cells, Rat1A cells, NRK cells, and NIH3T3 cells were transfected with constitutively active or the dominant negative mutant of GFP-Rac1 and were analyzed to identify the multinucleated phenotype as in Fig. 4. *B*, cells were transfected with a plasmid encoding constitutively active Pak1, Pak1 T423E, and analyzed for the multinucleated phenotype. *Cont*, control.

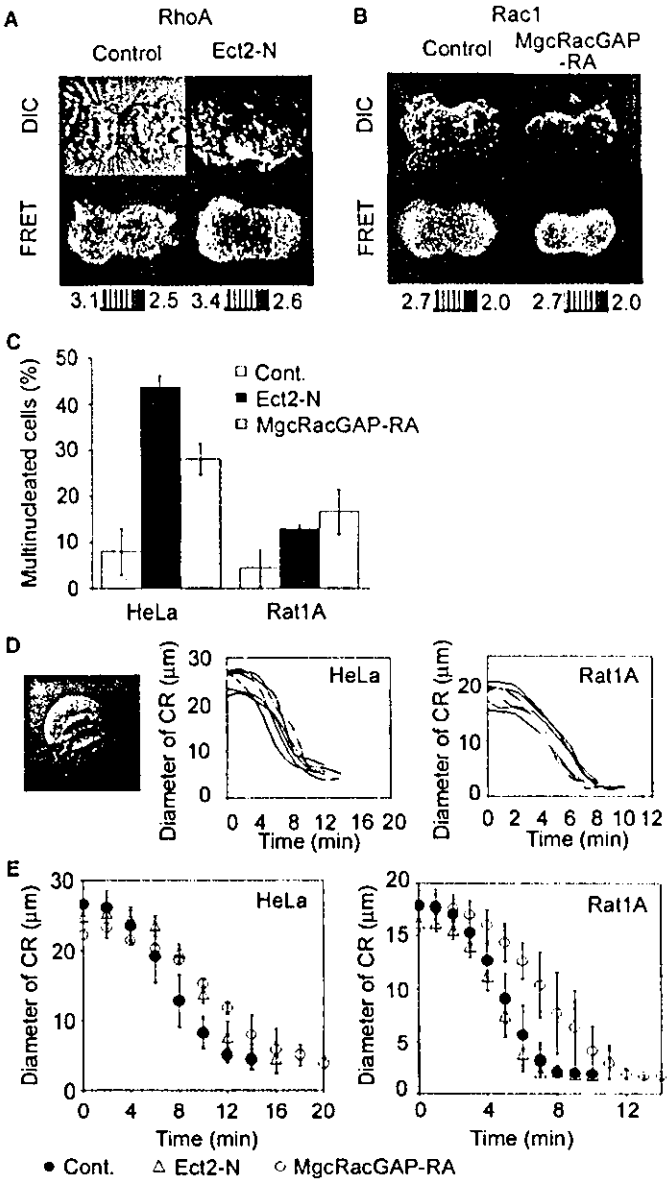

FIG. 6. **Effect of dominant negative mutants of Ect2 and MgcRacGAP/CYK-4.** *A*, HeLa cells expressing Ect2-N and Raichu-RhoA were imaged as in Fig. 2*A*. *B*, HeLa cells expressing MgcRacGAP-RA and Raichu-Rac1 were imaged as in Fig. 3*A*. *C*, HeLa cells and Rat1A cells were transfected with Ect2-N and MgcRacGAP-RA and were analyzed to identify the multinucleated phenotype as in Fig. 4. *D*, time-lapse analysis of cytokinesis in HeLa and Rat1A cells. The diameter of the contractile ring was measured as illustrated in the *left panel*. The *right panel* shows the aligned time courses of cleavage furrow constriction in control cells ($n = 10$). *E*, HeLa and Rat1A cells were mock-transfected or transfected with pEGFP-C1-Ect2-N4 or pEredMit-MgcRacGAP-RA and were observed for cytokinesis. *Cont.*, control. The averaged time courses are shown ($n = 4$).

5*B*). Thus, a decrease in Rac1 activity and the resulting suppression of Pak1 appear to be essential steps of cytokinesis in a variety of cell types.

Inhibition of Cytokinesis by Dominant Negative Mutants of Ect2 and MgcRacGAP/CYK-4—We further studied the mechanism of changes in the activity of Rho family GTPases during cytokinesis. For this purpose, we utilized dominant negative mutants of Ect2 and MgcRacGAP/CYK-4, which have been shown to regulate cytokinesis (18, 22, 23, 25). In cells expressing the dominant negative mutant of Ect2, Ect2-N, the increase in RhoA activity was suppressed at the cleavage furrow but not at the plasma membrane of polar sides (Fig. 6*A*). This observation agrees with the previously demonstrated recruitment of Ect2 to the cleavage furrow during cytokinesis (18) and suggests that multiple Rho GEFs are activated during cytokinesis. In cells expressing the dominant negative mutant of MgcRacGAP, MgcRacGAP-RA, Rac1 activity was not decreased at the cleavage furrow of HeLa cells, indicating that the suppression of Rac1 activity during cytokinesis was primarily mediated by the recruitment of MgcRacGAP (Fig. 6*B*).

To determine the effect of these mutants on cytokinesis quantitatively, we scored the number of multinucleated cells in the presence or absence of GFP-Ect2-N or MgcRacGAP-RA (Fig. 6*C*). Both GFP-Ect2-N and MgcRacGAP-RA increased the number of the multinucleated cells in HeLa cells. The effect of these mutants on Rat1A cells was marginal in this assay. Therefore, to examine the effect of these mutants on cytokinesis more directly, we measured the diameter of the contractile ring as shown by DIC images created during cytokinesis, and we calculated the maximum velocity of its shortening and the half-time of cytokinesis. The half-life of the shortening of the contractile ring was 7.2 min in the HeLa cells and 4.7 min in the Rat1A cells (Fig. 6*D*). In the presence of GFP-Ect2-N and MgcRacGAP-RA, the half-life of the shortening of the contractile ring was increased to 9.6 and 11.2 min, respectively, in HeLa cells (Fig. 6*E*). In Rat1A cells, however, only MgcRacGAP-RA increased the half-life of the contractile ring shortening to 7.1 min. These observations suggest the following conclusions. First, the increase in RhoA activity at the cleavage

furrow of HeLa cells was primarily mediated by Ect2. Second, the decrease in Rac1 activity at the cleavage furrow was primarily mediated by MgcRacGAP. Third, the activation of RhoA was not essential for the cytokinesis of Rat1A cells. Fourth, in Rat1A cells, suppression of Rac1 plays a more critical role in cytokinesis than activation of RhoA.

Recently, it has been shown that increases in RhoA activity are responsible for cortical rigidity (35). Diffuse increases in RhoA activity at the plasma membrane may play a role in this increased cortical rigidity. However, the results obtained with GFP-Ect2-N seem to indicate that such an increase at the cortex is not sufficient for cytokinesis, unless it is accompanied by an increase in RhoA activity at the cleavage furrow. More importantly, these results demonstrated that the inhibition of cytokinesis by C3 or GFP-Ect2-N in each cell type was closely correlated with an increase in RhoA activity during cytokinesis, as observed by the Raichu probes used here.

Notably, our observations are not necessarily in conflict with the recent finding that MgcRacGAP/CYK-4 phosphorylated by Aurora B acts on RhoA at the time of the abscission of daughter cells (24, 25). Because of the limitation in the resolution of the FRET images, we were unable to conclude whether or not RhoA was suppressed at the spindle midbody at the time of abscission.

Role of ROCK and MLCK on the Cytokinesis of HeLa and Rat1A Cells—To understand further the role of Rho family GTPases in the cytokinesis of HeLa and Rat1A cells, we tested the effects of various inhibitors that have been shown to disturb cytokinesis. First, we tested the effects of blebbistatin, an inhibitor of myosin II (36), because cytokinesis can proceed in a myosin II-independent manner in *Dictyostelium discoideum* (37). As shown in Fig. 7, blebbistatin abrogated the cytokinesis of both HeLa and Rat1A cells. Thus, we proceeded to examine the contribution of ROCK and MLCK, which can induce actomyosin contraction by the phosphorylation of the light chain of myosin II (2). To this end, we treated the cells with Y27632, an inhibitor of ROCK, or ML-7, an inhibitor of MLCK. In HeLa cells, the effect of ML-7 was insignificant, whereas Y-27632 markedly delayed the velocity of cleavage furrow ingression, as reported previously (38). In contrast, ML-7, but not Y27632 significantly inhibited the cleavage furrow ingression of Rat1A cells. Therefore, a relief of Pak suppression seemed to lead to MLCK-promoted cytokinesis in Rat1A cells, as suggested previously (6). One of our co-authors (39) has recently reported an essential role of MLCK in the normal spindle morphology and chromosomal alignment of mitotic HeLa cells by using dominant negative mutants of MLCK. In these HeLa cells expressing the dominant negative MLCK mutants, the frequency of the multinucleated cells was up to 11%, whereas the percentage of multinucleated cells exceeded 50% in the presence of C3 (Fig. 4). In addition, the effect of the dominant negative mutants of MLCK on the velocity of cleavage furrow ingression was markedly weaker than that of Y-27632 (supplemental figure). Therefore, we concluded that the effect on MLCK was prominent in metaphase but less remarkable during cytokinesis in HeLa cells. Altogether, cytokinesis of HeLa cells seems to be more resistant to the inhibition of MLCK than Rat1A cells.

In conclusion, this study revealed that there are at least two pathways leading to actomyosin contraction and the resulting constriction of the cleavage furrow. The contribution of each pathway may depend on the cellular context. For example, the Ect2-RhoA-ROCK pathway is predominant in HeLa cells, whereas the MgcRacGAP/CYK-4-Rac1-Pak-MLCK pathway plays a more important role in the cytokinesis of Rat1A cells. Such differences in the mechanism of cytokinesis may in turn have generated the observed discrepancy in the requirement of RhoA for cytokinesis.

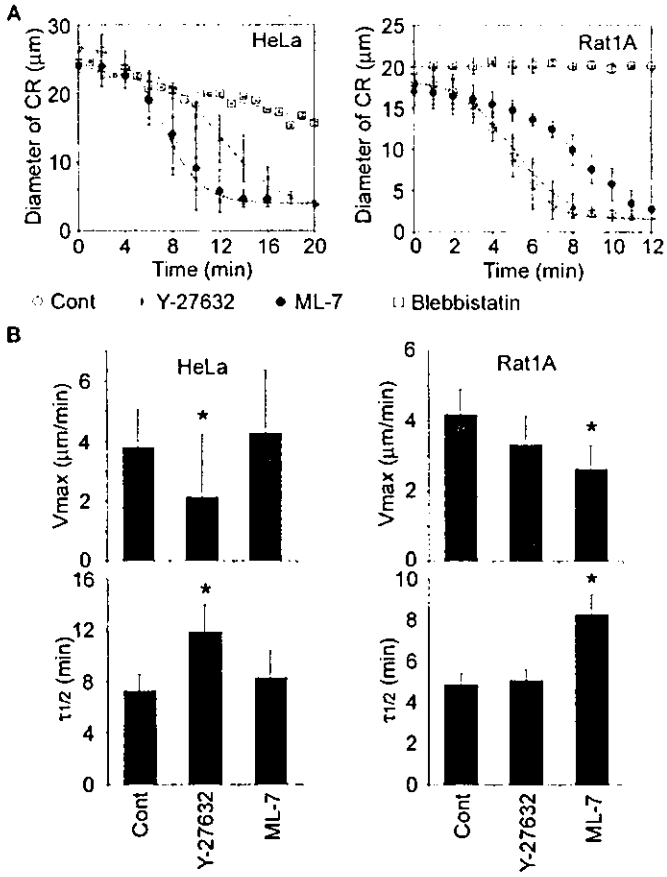

FIG. 7. **Differential role of ROCK and MLCK on the cytokinesis of HeLa and Rat1A cells.** *A*, HeLa and Rat1A cells untreated or treated with Y-27632, ML-7, or blebbistatin were observed for cytokinesis, as described in Fig. 6. The averaged time courses are shown ($n > 6$). *Cont.*, control. *B*, each time course was fitted to an exponential curve with GraFit software, by which the maximum velocity and the half-time ($\tau_{1/2}$) of cleavage furrow contraction were calculated; the results are shown as the mean ± S.D. *, $p < 0.005$ relative to the control.

Acknowledgments—We thank T. Miki, T. Kitamaura, H. Kurose, J. Miyazaki, Y. Nakabeppu, G. M. Bokoch, and H. Okayama for their provision of reagents, members of the Matsuda laboratory for helpful discussions, and N. Yoshida, N. Fujimoto, and Y. Matsuura for their technical assistance.

Note Added in Proof—Following acceptance of this manuscript, a complementary study was published that provides further genetic support for our proposal that MgcRacGAP/CYK-4/RacGAP50C suppresses Rac during cytokinesis (D'Avino, P. P., Savoian, M. S., and Glover, D. M. (2004) *J. Cell Biol.* **166**, 61–71).

REFERENCES

1. Mabuchi, I. (1986) *Int. Rev. Cytol.* **101**, 175–213
2. Glotzer, M. (2001) *Annu. Rev. Cell Dev. Biol.* **17**, 351–386
3. Glotzer, M. (2004) *J. Cell Biol.* **164**, 347–351
4. Bishop, A. L., and Hall, A. (2000) *Biochem. J.* **348**, 241–255
5. Prokopenko, S. N., Saint, R., and Bellen, H. J. (2000) *J. Cell Biol.* **148**, 843–848
6. Mandato, C. A., Benink, H. A., and Bement, W. M. (2000) *Cell Motil. Cytoskeleton* **45**, 87–92
7. Drechsel, D. N., Hyman, A. A., Hall, A., and Glotzer, M. (1997) *Curr. Biol.* **7**, 12–23
8. Kishi, K., Sasaki, T., Kuroda, S., Itoh, T., and Takai, Y. (1993) *J. Cell Biol.* **120**, 1187–1195
9. Mabuchi, I., Hamaguchi, Y., Fujimoto, H., Morii, N., Mishima, M., and Narumiya, S. (1993) *Zygote* **1**, 325–331
10. Amano, M., Ito, M., Kimura, K., Fukata, Y., Chihara, K., Nakano, T., Matsuura, Y., and Kaibuchi, K. (1996) *J. Biol. Chem.* **271**, 20246–20249
11. Kosako, H., Yoshida, T., Matsumura, F., Ishizaki, T., Narumiya, S., and Inagaki, M. (2000) *Oncogene* **19**, 6059–6064
12. Yamashiro, S., Totsukawa, G., Yamakita, Y., Sasaki, Y., Madaule, P., Ishizaki, T., Narumiya, S., and Matsumura, F. (2003) *Mol. Biol. Cell* **14**, 1745–1756
13. O'Connell, C. B., Wheatley, S. P., Ahmed, S., and Wang, Y. L. (1999) *J. Cell Biol.* **144**, 305–313
14. Dutartre, H., Davoust, J., Gorvel, J. P., and Chavrier, P. (1996) *J. Cell Sci.* **109**, 367–377
15. Muris, D., Verschoor, T., Divecha, N., and Michalides, R. (2002) *Eur. J. Cancer*

38, 1775–1782
16. Sanders, L. C., Matsumura, F., Bokoch, G. M., and de Lanerolle, P. (1999) *Science* **283,** 2083–2085
17. Prokopenko, S. N., Brumby, A., O'Keefe, L., Prior, L., He, Y., Saint, R., and Bellen, H. J. (1999) *Genes Dev.* **13,** 2301–2314
18. Tatsumoto, T., Xie, X., Blumenthal, R., Okamoto, I., and Miki, T. (1999) *J. Cell Biol.* **147,** 921–928
19. Mishima, M., and Glotzer, M. (2003) *Curr. Biol.* **13,** R589–R591
20. Somers, W. G., and Saint, R. (2003) *Dev. Cell* **4,** 29–39
21. Jantsch-Plunger, V., Gonczy, P., Romano, A., Schnabel, H., Hamill, D., Schnabel, R., Hyman, A. A., and Glotzer, M. (2000) *J. Cell Biol.* **149,** 1391–1404
22. Hirose, K., Kawashima, T., Iwamoto, I., Nosaka, T., and Kitamura, T. (2001) *J. Biol. Chem.* **276,** 5821–5828
23. Mishima, M., Kaitna, S., and Glotzer, M. (2002) *Dev. Cell* **2,** 41–54
24. Minoshima, Y., Kawashima, T., Hirose, K., Tonozuka, Y., Kawajiri, A., Bao, Y. C., Deng, X., Tatsuka, M., Narumiya, S., Muy, W. S., Nosaka, T., Semba, K., Inoue, T., Satoh, T., Inagaki, M., and Kitamura, T. (2003) *Dev. Cell* **4,** 549–560
25. Lee, J. S., Kamijo, K., Ohara, N., Kitamura, T., and Miki, T. (2004) *Exp. Cell Res.* **293,** 275–282
26. Ban, R., Irino, Y., Fukami, K., and Tanaka, H. (2004) *J. Biol. Chem.* **279,** 16394–16402
27. Itoh, R. E., Kurokawa, K., Ohba, Y., Yoshizaki, H., Mochizuki, N., and Matsuda, M. (2002) *Mol. Cell. Biol.* **22,** 6582–6591
28. Yoshizaki, H., Ohba, Y., Kurokawa, K., Itoh, R. E., Nakamura, T., Mochizuki, N., Nagashima, K., and Matsuda, M. (2003) *J. Cell Biol.* **162,** 223–232
29. Sells, M. A., Knaus, U. G., Bagrodia, S., Ambrose, D. M., Bokoch, G. M., and Chernoff, J. (1997) *Curr. Biol.* **7,** 202–210
30. Miyawaki, A., Llopis, J., Heim, R., McCaffery, J. M., Adams, J. A., Ikura, M., and Tsien, R. Y. (1997) *Nature* **388,** 882–887
31. Welsh, C. F., Roovers, K., Villanueva, J., Liu, Y., Schwartz, M. A., and Assoian, R. K. (2001) *Nat. Cell Biol.* **3,** 950–957
32. Rooney, R. D., Tuazon, P. T., Meek, W. E., Carroll, E. J., Hagen, J. J., Gump, E. L., Monnig, C. A., Lugo, T., and Traugh, J. A. (1996) *J. Biol. Chem.* **271,** 21498–21504
33. Bokoch, G. M. (2003) *Annu. Rev. Biochem.* **72,** 743–781
34. Poperechnaya, A., Varlamova, O., Lin, P. J., Stull, J. T., and Bresnick, A. R. (2000) *J. Cell Biol.* **151,** 697–708
35. Maddox, A. S., and Burridge, K. (2003) *J. Cell Biol.* **160,** 255–265
36. Straight, A. F., Cheung, A., Limouze, J., Chen, I., Westwood, N. J., Sellers, J. R., and Mitchison, T. J. (2003) *Science* **299,** 1743–1747
37. Gerisch, G., and Weber, I. (2000) *Curr. Opin. Cell Biol.* **12,** 126–132
38. Kosako, H., Goto, H., Yanagida, M., Matsuzawa, K., Fujita, M., Tomono, Y., Okigaki, T., Odai, H., Kaibuchi, K., and Inagaki, M. (1999) *Oncogene* **18,** 2783–2788
39. Dulyaninova, N. G., Patskovsky, Y. V., and Bresnick, A. R. (2004) *J. Cell Sci.* **117,** 1481–1493

THE JOURNAL OF BIOLOGICAL CHEMISTRY
Vol. 279, No. 25, Issue of June 18, pp. 26274–26279, 2004
Printed in U.S.A.

Regulatory Roles for APJ, a Seven-transmembrane Receptor Related to Angiotensin-type 1 Receptor in Blood Pressure *in Vivo**

Received for publication, April 14, 2004
Published, JBC Papers in Press, April 15, 2004, DOI 10.1074/jbc.M404149200

Junji Ishida‡§, Tatsuo Hashimoto‡§¶, Yasumi Hashimoto‡§, Shiro Nishiwaki‡§, Taku Iguchi‡§, Shuichi Harada‡§, Takeshi Sugaya‡§, Hitomi Matsuzaki‡§, Rie Yamamoto‡§, Naotaka Shiota‖, Hideki Okunishi‖, Minoru Kihara¶, Satoshi Umemura¶, Fumihiro Sugiyama‡‡, Ken-ichi Yagami**‡‡, Yoshitoshi Kasuya§§, Naoki Mochizuki¶¶, and Akiyoshi Fukamizu‡§‖‖**

*From the ‡Center for Tsukuba Advanced Research Alliance, §Institute of Applied Biochemistry, **Institute of Basic Medical Sciences, ‡‡Laboratory Animal Resource Center, University of Tsukuba, Tsukuba, Ibaraki 305-8577, Japan, the ¶Department of Internal Medicine II, Yokohama City University School of Medicine, Yokohama, Kanagawa 236-0004, Japan, the ‖Department of Pharmacology, Shimane University School of Medical, Izumo, Shimane 693-8501, Japan, the §§Department of Biochemistry and Molecular Pharmacology, Graduate School of Medicine, Chiba University, 1-8-1 Inohana, Chuo-ku, Chiba 260-8670, Japan, and the ¶¶Department of Structural Analysis, National Cardiovascular Center Research Institute, Suita, Osaka 565-8565, Japan*

APJ is a G-protein-coupled receptor with seven transmembrane domains, and its endogenous ligand, apelin, was identified recently. They are highly expressed in the cardiovascular system, suggesting that APJ is important in the regulation of blood pressure. To investigate the physiological functions of APJ, we have generated mice lacking the gene encoding *APJ*. The base-line blood pressure of APJ-deficient mice is equivalent to that of wild-type mice in the steady state. The administration of apelin transiently decreased the blood pressure of wild-type mice and a hypertensive model animal, a spontaneously hypertensive rat. On the other hand, this hypotensive response to apelin was abolished in APJ-deficient mice. This apelin-induced response was inhibited by pretreatment with a nitric-oxide synthase inhibitor, and apelin-induced phosphorylation of endothelial nitric-oxide synthase in lung endothelial cells from APJ-deficient mice disappeared. In addition, APJ-deficient mice showed an increased vasopressor response to the most potent vasoconstrictor angiotensin II, and the base-line blood pressure of double mutant mice homozygous for both APJ and angiotensin-type 1a receptor was significantly elevated compared with that of angiotensin-type 1a receptor-deficient mice. These results demonstrate that APJ exerts the hypotensive effect *in vivo* and plays a counterregulatory role against the pressor action of angiotensin II.

A family of G protein-coupled receptors bind a large variety of ligands and plays an essential role for physiological functions *in vivo* including the maintenance of homeostasis in the cardiovascular system. *APJ* (a putative receptor protein related to the angiotensin-type 1 receptor (AT1))[1] is a G protein-coupled receptor that was isolated from human genomic DNA using the polymerase chain reaction (1). The *APJ* has a 31% amino acid sequence homology with the AT1, but APJ does not display specific binding for angiotensin II, which is the ligand of AT1 and exerts a pressor action in the blood pressure regulation (1). Recently, the endogenous ligand of APJ was identified from bovine stomach, and this peptide was named apelin (for APJ endogenous ligand) (2). APJ and apelin are expressed in several tissues including the cardiovascular and the central nervous systems (3–6), and the structure of APJ and apelin is highly conserved among species, suggesting its important physiological roles.

Intravenous administration of apelin suggested a hypotensive effect in rat (5, 7–9). On the other hand, apelin potently contracts human saphenous vein smooth muscle cells *in vitro* (10), indicating that apelin is a potent vasoconstrictor. Thus, at this moment, the action of apelin in blood pressure regulation is controversial, and it is still unclear whether these actions of apelin are really through APJ because of the absence of specific receptor blocker to clarify the *in vivo* functions of APJ. Therefore, in this study, by using animal models such as APJ-deficient mice, APJ/AT1a double knock-out mice, and spontaneously hypertensive rat and by using endothelial cells from mice, we evaluated the functional importance of apelin-APJ signaling in the blood pressure regulation *in vitro* and *in vivo*.

EXPERIMENTAL PROCEDURES

Gene Targeting and Generation of Mutant Mice—The genomic DNA containing the *APJ* locus were isolated from a phage library from C57BL/6 mice (11) with the human *AT1* cDNA as a probe. To construct a targeting vector for the *APJ* gene, the 156-bp fragment of the mouse *APJ* gene between the NcoI site including the translation initiation codon of the gene and the Csp45I site was replaced with the nuclear localization signal-*lacZ* cassette. The neomycin phosphotransferase (*neo*) gene cassette derived from pMC1neoPolyA (Stratagene) was placed downstream of the nuclear localization signal-*lacZ* gene. The

* This work was supported in part by the 21st Century COE Program, "Research for the Future" Program (The Japan Society for the Promotion of Science Grant JSPS-RFTF 97L00804), a grant-in-aid for Scientific Research on Priority Areas, a grant-in-aid for Scientific Research (A) and a grant-in-aid for Young Scientists (B) from the Ministry of Education, Culture, Sports, Science and Technology of Japan, Research Grant 11C-1 for Cardiovascular Diseases, a grant for Comprehensive Research on Aging and Health from the Ministry of Health, Labor, and Welfare of Japan, the University of Tsukuba Special Research Program, Japan Heart Foundation Research Grant, The Nissan Science Foundation, and Suzuken Memorial Foundation. The costs of publication of this article were defrayed in part by the payment of page charges. This article must therefore be hereby marked "*advertisement*" in accordance with 18 U.S.C. Section 1734 solely to indicate this fact.

‖‖ To whom correspondence should be addressed: Center for Tsukuba Advanced Research Alliance, Institute of Applied Biochemistry, University of Tsukuba, Ibaraki 305-8577, Japan. Tel./Fax: 81-298-53-6070; E-mail: akif@tara.tsukuba.ac.jp.

[1] The abbreviations used are: AT1, angiotensin-type 1 receptor; WKY, Wistar-Kyoto; SHR, spontaneously hypertensive rat; DMEM, Dulbecco's modified Eagle's medium; NO, nitric oxide; eNOS, endothelial NO synthase; L-NAME, N^G-nitro-L-arginine methyl ester.

6.3-kb XhoI/NcoI fragment and the 1.6-kb Csp45I/Sau3AI fragment of the *APJ* gene were included upstream and downstream of these cassettes, respectively (Fig. 1*A*). Details of the negative selection with the diphtheria toxin-A cassette are described elsewhere (12). The TT2 ES cells were grown on embryonic fibroblast feeder cells as described previously (13). Homologous recombination in TT2 ES cells was detected by Southern blotting using probe a (687-bp BanIII-Sau3AI fragment). Chimeric mice were generated by injecting the ES cells into ICR 8-cell embryos (13, 14). AT1a-deficient mice were generated as described previously (11). Double knock-out mice for *APJ* and *AT1a* used in this study were generated from heterozygous mice after the crossing of single APJ-deficient and AT1a-deficient mice.

RNA Preparation and Northern Blot Analysis—Total RNA was isolated from the heart and lung of four independent age-matched mice using ISOGEN (NipponGene) (15). Fifteen micrograms of RNA were denatured with glyoxal, separated by electrophoresis, and transferred to a nylon membrane. The 728-bp NcoI/NaeI fragment that corresponds to the coding regions of *APJ* was used as the APJ receptor-specific probe (probe b). Probes for mouse glyceraldehyde-3-phosphate dehydrogenase were described previously (16).

Measurement of Blood Pressure—The heart rate and systolic, mean, and diastolic blood pressures were measured by a programmable sphygmomanometer (BP-200, Softron, Japan) using the tail cuff method as described previously (17). Unanesthetized mice were introduced into a holder mounted in a thermostatically controlled warming plate and maintained at 37 °C during measurement.

Intraperitoneal Injection of Apelin—Experiments were performed using 4-month-old male mice under the conscious and unrestrained conditions. [Pyr^1]Apelin-13 (Peptide Institute 4361-v) was suspended in saline (0.9% NaCl in distilled water). After the measurement of the basal systolic blood pressure, [Pyr^1]apelin-13 was administered by intraperitoneal injection at 285 μg/kg body weight and the systolic blood pressure was measured continuously. The data were calculated at 5-min intervals for 20 min after the administration of apelin.

Intravenous Injection of Apelin in Wistar-Kyoto (WKY) Rat and SHR—SHR and WKY rats at 12 weeks of age were anesthetized with sodium pentobarbital (35 mg/kg intraperitoneal). PE-10 catheters (Clay Adams, Parsippany, NJ) were inserted into the right femoral artery for measuring blood pressure and into the right femoral vain for allowing the administration of [Pyr^1]apelin-13. The arterial catheter was connected to a pressure transducer (TP-200T, Nihon Kohden, Tokyo, Japan), and blood pressure was measured continuously. The anesthetic level was maintained by subcutaneous injection of 10 mg/kg pentobarbital every 40 min. [Pyr^1]Apelin-13 dissolved in 0.1 ml of saline was administered through the vein catheter (2, 4, and 10 nmol/kg).

Pretreatment with N^G-Nitro-L-Arginine Methyl Ester (L-NAME) and Intraperitoneal Injection of Apelin in Wild-type and APJ-deficient Mice—Experiments were performed using 4-month-old male mice under the conscious and unrestrained conditions. L-NAME (Sigma) was suspended in saline. Systolic blood pressure was continuously measured before and after acute intraperitoneal injection of L-NAME (10 mg/kg body weight). At 15 min after the administration of L-NAME, the additional administration of [Pyr^1]apelin-13 (285 μg/kg body weight) or saline alone was performed by intraperitoneal injection and the systolic blood pressure was measured continuously. The maxima of systolic blood pressure responses to injections of apelin were calculated in a 0–5 min-post-injection of apelin.

Preparation of Endothelial Cells from Wild-type and APJ-deficient Mice—The lung of wild-type and APJ-deficient male mice at 11 weeks of age was perfused with 0.25% heparin/phosphate-buffered saline(−) and removed aseptically, rinsed in 0.25% heparin/phosphate-buffered saline(−), minced into ~1 × 2-mm squares, and digested in 20 ml of collagenase type I (4 mg/ml, Worthington) in serum-free DMEM containing antibiotic at 37 °C for 60 min with shaking. The cellular digest was filtered through a sterile 40-μm nylon mesh and washed in 20 ml of serum-free DMEM, and the cell pellet was resuspended in 4 ml of serum-free DMEM. 2 ml of cell suspension were put into the tube containing 12 ml of 30% Percoll and centrifuged at 800 × *g* for 15 min. 2 ml of the concentrated fraction with the endothelial cells were recovered to which 2 ml of serum-free DMEM were added, and then the Percoll density gradient centrifugation was carried out again. The collected endothelial cells then were resuspended in 4 ml of growth medium (DMEM containing 10% fetal bovine serum and endothelial cell growth supplement from bovine neural tissue (Sigma)) for culture. Contaminated vascular smooth muscle cells were stripped off physically as necessary. Confluent cells were passed routinely at a split ratio of 1–3 after trypsin/EDTA digestion and cultured under the same conditions. We ascertained the purity of endothelial cells by Western blotting with monoclonal anti-mouse CD-31 antibody (BD Biosciences) (data not shown).

Detection of Endothelial NO Synthase (eNOS) Phosphorylation—Isolated endothelial cells from wild-type and APJ-deficient mice were cultured in 6-well plates and stimulated by [Pyr^1]apelin-13 (10 μM) or fetal bovine serum (10%) for 5 min, and the reaction was terminated by adding Laemmli buffer. The cell lysates were subjected to SDS/7.5% polyacrylamide gel electrophoresis and then transferred to polyvinylidene difluoride membrane (Millipore). After blocking with a blocking buffer containing 5% milk, the membrane was incubated with a polyclonal anti-human phospho-eNOS (Ser^{1177}) antibody (Cell Signaling Technology) and bound antibody was detected by horseradish peroxydase-labeled donkey anti-(rabbit IgG) serum (Amersham Biosciences) using Western Lightning Plus chemiluminescence reagents (Perkin-Elmer Life Sciences) to measure the phosphorylation of eNOS. After washing with a reprobing buffer of the composition (62.5 mM Tris-HCl (pH 6.7), 100 mM β-mercaptoethanol, and 2% SDS), the same membrane was subjected to Western blotting with a monoclonal anti-eNOS antibody (BD Transduction Laboratories) to detect the expression levels of eNOS as an internal control.

Treatment with Captopril and Intraperitoneal Injection of Angiotensin II—Systolic blood pressure was measured in conscious and unrestrained female mice at 4 months of age as mentioned above. The basal systolic blood pressure and the pressure responses against intraperitoneal injection of angiotensin II (10 and 30 μg/kg) were measured prior to the administration of captopril. After the administration of captopril (500 mg/liter in drinking water) for 1 week to inhibit the endogenous production of angiotensin II, the pressure responses to angiotensin II given from lower dose (3–30 μg/kg) were recorded continuously for 40 min after the administration of angiotensin II.

Statistical Analysis—The data were analyzed by Student's *t* test for unpaired values. $p < 0.05$ was considered significant. Results are expressed as the means ± S.E.

RESULTS AND DISCUSSION

Generation of APJ-deficient Mice—To generate a null mutation at the mouse *APJ* gene locus, we designed a targeting vector that would replace a portion of the *APJ* coding region with the promoterless *lacZ* gene (Fig, 1*A*). After electroporation of TT2 cells with the targeting vector, homologous recombination was confirmed by Southern blotting (Fig. 1*B*, *left panel*). 10 independent cell lines of 195 G418-resistant cells had undergone homologous recombination at the mouse *APJ* locus. Eight clones were injected into ICR 8-cell embryos to generate chimeric mice, and two clones gave rise to germ line transmission by backcross mating with C57BL/6J mice. The heterozygous mice were intercrossed to produce homozygous offspring, and the mutation at *APJ* loci was detected by Southern analysis of tail DNA (Fig. 1*B*, *right panel*). Of the 396 offspring analyzed, 76 (19%) were homologous for the disrupted allele and 103 (26%) were wild type, indicating the normal embryonic development of the homozygous mutant mice. The histological sections of heart, lung, kidney, spleen, brain, ovary, skeletal muscle, liver, and white adipose did not reveal any differences in morphology between wild-type and heterozygous or homozygous mutant mice (data not shown). In the following study, to gain the equivalent effects of other gene backgrounds with the exception of for the *APJ* gene, we used these intercrossed littermates of heterozygous mice for further physiological experiments.

RNA Analysis—To determine whether *APJ* message was present in homozygous mutants, we performed Northern blot analysis of heart and lung RNA. Although heart and lung highly express the *APJ* gene in rodents (3), homozygous mutant mice had no detectable *APJ* message (Fig. 1*C*). A duplicate blot was analyzed with a glyceraldehyde-3-phosphate dehydrogenase probe to confirm that the RNA sample was intact. These results indicated that *APJ* transcripts were absent completely from homozygous mutant mice (APJ-deficient mice).

Measurement of Blood Pressure and Administration of Apelin—To ascertain whether APJ-mediated pathways participate in the regulation of the cardiovascular system, we measured the systolic blood pressure and heart rate under the steady

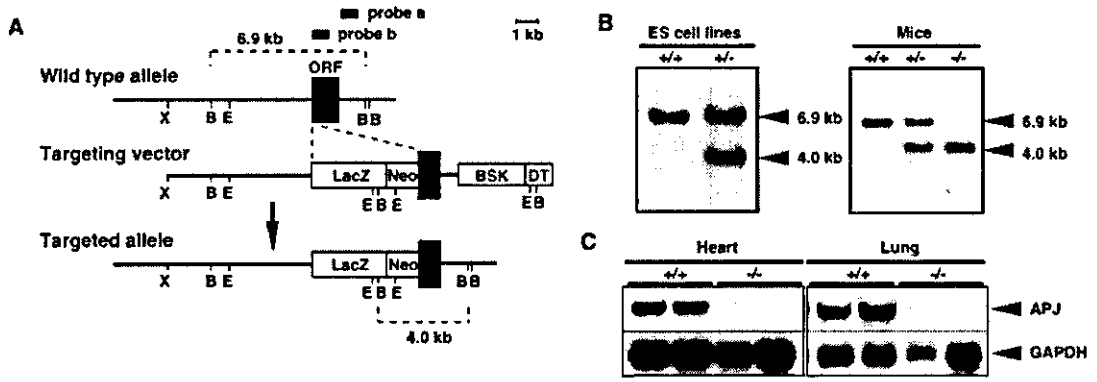

FIG. 1. **Targeted disruption of the mouse APJ gene by homologous recombination in ES cells and mice.** *A*, structure of the targeting vector and partial restriction map of the mouse APJ gene locus before and after targeting event. The intronless open reading frame (*ORF*) is shown as a *closed box*, and the nuclear localization signal-β-galactosidase gene (*LacZ*), the neomycin phosphotransferase gene (*Neo*), the diphtheria toxin-A gene (*DT*), and pBluescript II (*BSK*) are shown as an *open box*. The position of the probes used for Southern blot analysis (*closed bar*) is also shown. The restriction sites used are: *B*, BamHI; *E*, EcoRI; *X*, XhoI. *B*, Southern blot analyses of ES cell (*left panel*) and representative litter derived from a heterozygous intercross (*right panel*). Genomic DNAs isolated from wild type (+/+) and targeted (+/−) ES cell clones and from tails of wild-type (+/+), heterozygous (+/−), and homozygous (−/−) APJ mutant mice were digested with BamHI, electrophoresed, and blotted. Fragments obtained from wild type (6.9 kb) and targeted alleles (4.0 kb) were detected by *probe a*. *C*, Northern blot analysis of APJ-deficient mice. RNA samples from heart and lung of wild-type (+/+) and homozygous (−/−) mutant mice were electrophoresed and subjected to Northern blot analysis with probes for mouse APJ (*probe b*) and glyceraldehyde-3-phosphate dehydrogenase.

state. As shown in Fig. 2*A*, APJ-deficient mice and wild-type mice did not show any difference in the base-line systolic blood pressure (106.7 ± 2.0 and 105.9 ± 2.5 mm Hg, respectively) and the heart rate (632.0 ± 19.2 and 616.1 ± 32.8 cpm, respectively), suggesting that APJ is not essential for the maintenance of base-line blood pressure. Furthermore, it is reported that apelin is concerned in the regulation of drinking behavior (5, 7, 18), but the volume of water intake and the concentration of urinary electrolytes of APJ-deficient mice are not distinguishable from those of wild-type littermates when water is freely available (data not shown).

It has been reported that blood pressure was decreased transiently by the systemic administration of apelin, the endogenous ligand of APJ, in rat (5, 7–9). We administered apelin to APJ-deficient mice to ascertain whether these actions of apelin are really through APJ. Apelin is derived from a 77-amino acid precursor and processed to several isoforms by deleting the amino terminus (3, 4). The pyroglutamylated form of apelin-13, [pGlu]apelin-13, has been reported to have the effective activity at the receptor *in vitro* (3). Conscious male mice were intraperitoneally injected with [pGlu]apelin-13. The acute administration of apelin transiently and significantly decreased in the systolic blood pressure of wild-type mice (Fig. 2*B*). On the other hand, the apelin injection revealed no change in systolic blood pressure of APJ-deficient mice (Fig. 2*C*) without a change in heart rate as well as that of wild-type mice (data not shown). These results clearly demonstrate that the systemic administration of apelin lowers the blood pressure in wild-type but not in APJ-deficient mice and that APJ is really responsible for this action of apelin on the blood pressure regulation.

Administration of Apelin to Spontaneously Hypertensive Rat—Given that the activation of the apelin-APJ signaling pathways lowers the blood pressure under the steady state in mice (Fig. 2*B*) and rats (5, 7–9), is the hypotensive effect also evoked in the hypertensive conditions? To address this question, we administered apelin intravenously to a chronic hypertensive model animal, SHR, and measured continuously the arterial blood pressure. WKY rats were used as a control. Before the administration of apelin, the base-line mean blood pressure of WKY rats and SHR was measured (77 ± 4 mm Hg, n = 10, and 117 ± 2 mm Hg, n = 9, respectively). When apelin was injected into the normotensive WKY rats, a dose-dependent and significant decrease in mean arterial blood pressure was elicited (Fig. 2*D*, *closed bar*) as reported previously (5, 7–9). The intravenous administration of apelin to SHR was found to significantly lower the mean arterial blood pressure in a dose-dependent manner (Fig. 2*D*, *open bar*). Thus, the hypotensive effect by the systemic administration of apelin was evoked in hypertensive animals, but the degree of decrement was less than that of WKY rats. The effects of apelin on blood pressure regulation in the hypertensive model animals have not been explored previously to date, although it has been recently reported that apelin-APJ signaling pathways were down-regulated in the mechanical stretch models *in vitro*, in the animal models of chronic ventricular pressure overload, and in patients with chronic heart failure *in vivo* (19–21). In addition, the angiotensin-converting enzyme-related carboxypeptidase (ACE2), a zinc metalloprotease whose closest homolog is the angiotensin I-converting enzyme, was identified as the breakdown enzyme for apelin peptides (22). The reduction of apelin-induced hypotensive effects in SHR compared with WKY rats might be attributed to the differences in the balance of the production and degradation of apelin and in the sensitivity of APJ-mediated intracellular signalings including receptor desensitization.

Effects of a Nitric Oxide Synthase Inhibitor on the Action of Apelin Administration—Tatemoto *et al.* (8) suggest that apelin causes vasodilatation via the activation of the nitric oxide (NO)/L-arginine system. NO generated by eNOS has a central role in the regulation of vascular tone. Therefore, we examined the effects of a nitric-oxide synthase inhibitor, L-NAME, against the depressor response of apelin-APJ signaling observed in wild-type mice. After a single intraperitoneal bolus injection (10 mg/kg body weight) of L-NAME, the systolic blood pressure increased similarly from 111.0 ± 2.2 to 142.3 ± 2.9 mm Hg and from 108.1 ± 2.4 to 142.4 ± 2.5 mm Hg in wild-type and APJ-deficient mice (n = 7–8/group), respectively. This increase in systolic blood pressure with the administration of L-NAME was described previously in rat, and the systolic blood pressure of each group reached a plateau at around 10 min after administration (data not shown). Accordingly, we injected the apelin peptide at 15 min after L-NAME administration. The injection of apelin induced an acute and transient decrease in systolic blood pressure in the non-treated wild-type mice. In contrast, the administration of the same dose of apelin caused almost no change in systolic blood pressure in wild-type mice pretreated